SMC Bulletin

ISSN 2394-5087

A Publication of the Society for Materials Chemistry

Volume 14 No. 2 August 2023

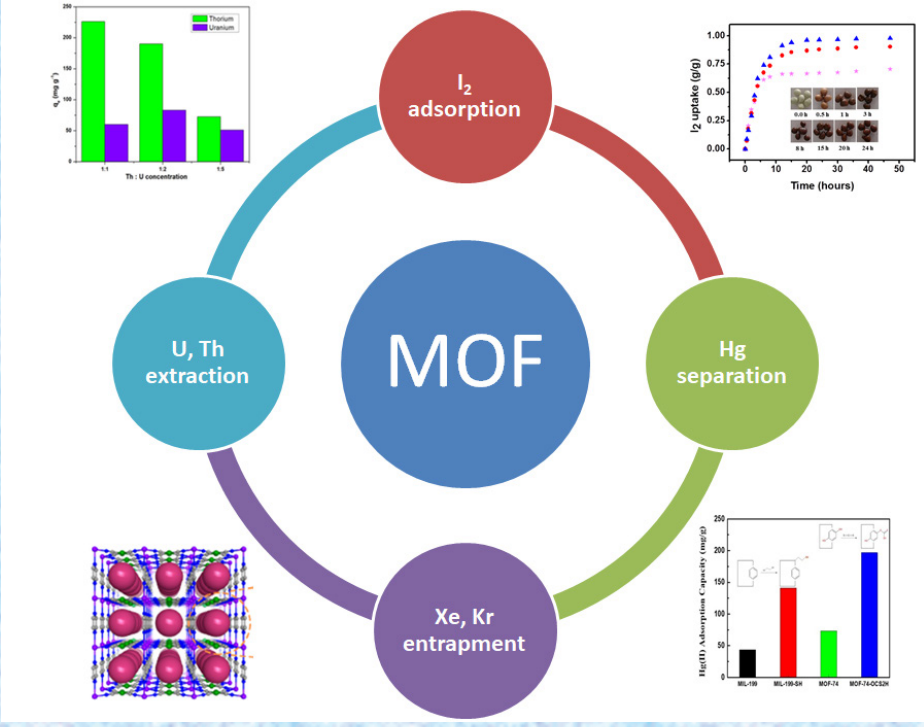

Special Issue on

Metal Organic Framework for Nuclear Application

SOCIETY FOR MATERIALS CHEMISTRY

Society for Materials Chemistry

Society for Materials Chemistry was mooted in 2007 with following aims and objectives:

(a) to help the advancement, dissemination and application of the knowledge in the field of materials chemistry,

(b) to promote active interaction among all material scientists, bodies, institutions and industries interested in achieving the advancement, dissemination and application of the knowledge of materials chemistry,

(c) to disseminate information in the field of materials chemistry by publication of bulletins, reports, newsletters, journals.

(d) to provide a common platform to young researchers and active scientists by arranging seminars, lectures, workshops, conferences on current research topics in the area of materials chemistry,

(e) to provide financial and other assistance to needy deserving researchers for participation to present their work in symposia, conference, etc.

(f) to provide an incentive by way of cash awards to researchers for best thesis, best paper published in journal/national/international conferences for the advancement of materials chemistry,

(g) to undertake and execute all other acts as mentioned in the constitution of SMC.

Executive Committee

Contact address
Society for Materials Chemistry
C/o Chemistry Division
Bhabha Atomic Research Centre, Trombay, Mumbai, 400 085, India
Tel: +91-22-25592001, E-mail: socmatchem@gmail.com

SMC Bulletin

A Publication of the Society for Materials Chemistry

Volume 14 No. 2 August 2023

Special Issue on

Metal Organic Framework for Nuclear Application

SOCIETY FOR MATERIALS CHEMISTRY

SMC Bulletin

Vol. 14 No. 2 August 2023

Guest Editor

Dr. Siddhartha Kolay
Chemistry Division
Bhabha Atomic Research Centre
Trombay, Mumbai - 400085
Email: siddhart@barc.gov.in

Published by

Society for Materials Chemistry
C/o. Chemistry Division
Bhabha Atomic Research Centre, Trombay, Mumbai, 400 085
E-mail: socmatchem@gmail.com,
Tel: +91-22-25592001

Guest Editorial

Dr. Siddhartha Kolay

As a promising alternative, nuclear energy is going to play a major role in coming decades to fulfill the world's energy demand. At present, ~ 11 % of total world's energy demand is contributed by nuclear. However, fuel fission products and fuel production byproducts contain radioactive nuclides such as $^{129/131}I$, ^{127}Xe, ^{85}Kr, ^{235}U, ^{137}Cs, ^{90}Sr, ^{99}Tc, ^{79}Se, etc, that exist in gaseous, ionic, and other forms. Proper partitioning and safe storage of these radioactive wastes are paramount for the successful growth of nuclear technology. Since long back, researchers have increasingly focused on the development of various adsorbents for their selective sequestration. In recent time, a new class of crystalline porous material, known as metal organic framework shows promising growth in this aspect. Because of many fascinating properties like high surface area and porosity, easy structural modification with various functional groups, metal organic frameworks play a significant role in nuclear segment also.

This issue is an attempt to review the contribution of metal organic frameworks (MOFs) towards nuclear applications. This issue of SMC bulletin presents a compilation of articles on metal organic frameworks in the area of heavy metal extraction and management of gaseous and volatile fission products (Xe, Kr, I & CH^{3I}).

It is my pleasure and great honor to serve as the guest editor for this special issue on "Metal Organic Framework based Materials for Nuclear Energy Application". I extended my sincere gratitude to Dr. A. K. Tyagi, President of SMC, and the all executive committee members for giving me this opportunity. I express my gratitude to all the authors for contributing their articles. I hope the readers will find the articles engaging and informative.

From the desks of the President and Secretary

Dr. A. K. Tyagi

Dr. Sandeep Nigam

Dear SMC Members, Colleagues and Readers,

Warm greetings from the Executive Council of the Society for Materials Chemistry (SMC)!

There has been continuous effort of our editorial team to bring out contemporary thematic issues. The multidisciplinary nature of these issues makes them relevant to the researchers of different scientific background. In the same direction, current issue entitled "Metal Organic Framework for Nuclear Application" is another marching step.

As the title express, this thematic issue deal with application of Metal Organic Framework for Nuclear Application. First two articles describe utilization of Metal Organic Frameworks Applied for Adsorption of Heavy Metal Ions and iodine respectively. Next chapter is dedicated for Separation, Capture and Sensing/Detection of Noble Radioactive Gases using MOF. The last chapter of this thematic collection also narrates application of functionalized MOFs as Highly Efficient Adsorbents for Aqueous Mercury ions.

We gratefully acknowledge Dr. Siddhartha Kolay who agreed to be the guest editor of this issue and put in efforts to bring out this special issue. We also acknowledge the efforts of all the contributing authors for submitting their informative articles. We also thank all the members of SMC for their continued support and cooperation in the growth of the Society for Materials Chemistry.

CONTENTS

Fascinating Field of Metal Organic Frameworks Applied for Adsorption of Heavy Metal Ions from Aqueous Solution

Nitin Gumber[a,b] and Rajesh V. Pai[a,b]
[a]*Fuel Chemistry Division, Bhabha Atomic Research Centre, Mumbai, India- 400085*
[b]*Homi Bhabha National Institute, Anushaktinagar, Mumbai, India- 400094*
Email: ngumber@barc.gov.in, rajeshvp@barc.gov.in

Abstract

The state of art in the field of Metal Organic Frameworks (MOFs)has witnessed an exponential surge in the recent years. Because of their favorable characteristics like variable pore size, high surface area and pore volume, MOFs have been utilized in diverse applications in fields such as catalysis, drug delivery, adsorption etc. making them industrial products. Of late MOFs have been exploited for removal of heavy metal ions for waste water remediation. This article briefly summaries different methodologies employed for synthesizing them, the dependence of pH and other parameters on adsorption characteristics of different heavy metal ions. Finally, some future perspective is provided anticipating the newcomers to develop interest in the field.

1. Introduction

With the ever increase in population, the urge for development of industries is rising at a rapid pace. The byproducts of these industries usually constitute heavy metal ions which are likely to affect human health and biosphere if present in excess. For eg. the presence of As above 10 µg/L is known to affect kidney and liver.[1] Similarly the occurrence of Cd above 5 µg/L is considered alarming by World Health Organization (WHO) as it is directly linked with osteomalacia, anemia and brain related issues.[2] Another class of heavy metals associated with nuclear industry such as U, Th etc. pose problems not only due to the chemo toxicity associated with them but also due to their radiotoxicity. WHO specifies a threshold limit of 30 µg/L to U.[3] Remediation of such water bodies where these radiotoxic metal ions are disposed need to be managed by employing suitable measures. The presence of different metal ions requires different techniques for effective managing of waste water and thus poses a great challenge for the separation scientists. Depending on the metal ion of interest, different methodologies have been applied which includes precipitation, ion exchange, adsorption, membrane based etc.[4, 5] Major drawback among most of the techniques described above includes cost factor, high energy utilization and generation of secondary waste. Adsorption is considered to be the best among them since it is relatively simpler technique, generates low secondary waste and is highly efficient and applicable for a wide range of metal ions.

The use of activated carbon, zeolites, clays etc. have been used widely in the literature for adsorption of heavy metal ions because of their ease of synthesis and relatively cheaper raw materials required.[6] However, the low adsorption capacity, complicated functionalization and less selective behavior towards a particular metal ion renders their limited practical applicability. Thus, the research for more advanced materials which are devoid of above limitations is being pursued since last few years.

The major driving force for the adsorption is the presence of highly active adsorption sites which are directly or indirectly linked with high surface area and pore volume. To tackle the above challenge, the search for advanced porous materials like Metal Organic Frameworks (MOFs), Covalent Organic Frameworks (COFs)[7], Porous Organic Polymers (POPs)[8] etc. has exploded as hot topics in last two decades. The advantages of above-mentioned materials include ease of functionalization, high surface area and pore volume, selective metal ion capture etc. POPs are usually synthesized through typical organic reactions like C-C coupling, polymerization etc. and are linked through strong covalent bonds. Even though POPs can be tuned to have varying porosity but due to their amorphous nature, their characterization is a difficult task which creates vulnerability in predicting the mechanism of adsorption. COFs are also formed through strong covalent interactions and the functionality can be induced on the reactant organic molecule but the synthesis of COFs is tedious and only limited methods are known which result into formation of imine or ester linkages.[9]

2. Metal Organic Frameworks (MOFs)

MOFs are hybrid materials made up of inorganic metal

ions and organic linkers giving rise to a 3-D crystalline framework with regularly spaced apertures. The topic came into limelight at the end of last century when Yaghi et. al. synthesized a divalent metal based MOF with benzene dicarboxylic acid as the linker and named it as MOF-5 with Langmuir surface area ~ 2900 m2g-1which was higher than any other material reported at that time.[10] The group became more active and renowned as they discovered the concept of Isoreticular chemistry in 2002 in which different size of linkers were used and the topology of the MOF remained same but the pore size varied depending on the length of the linker as shown in Fig. 1.[11] The properties which distinguish MOFs from conventional materials include stability and rigidity of framework, versatility of formation of MOFs using diverse starting materials, exceptionally high surface area and pore volume, post synthetic modification to induce selectivity etc. The possibility of combining different metal ions and linkers led to the discovery of abundant MOFs like HKUST-1, MOF-76, UiO-66, CAU-1, MOF-5, MIL-53, MOF-808, ZIFs etc.[12] Apart from using carboxylate based linkers nitrogen containing molecules like azolate compounds were also utilized to synthesize class of MOFs known as ZIFs. The geometry of MOFs can also be tuned depending on the connectivity of linker varying from ditopic to octatopic linkers. Thus the framework obtained through these linkers

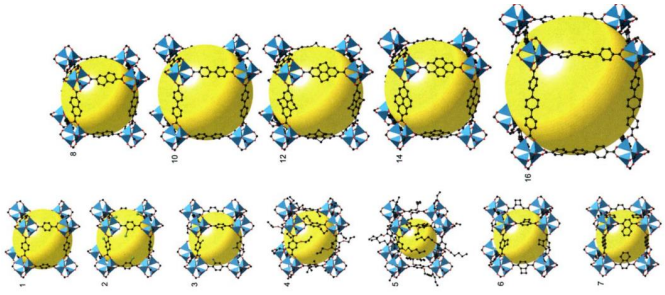

Fig. 1. *Single crystal x-ray structures of IRMOFs (Reproduced from ref. [11])*

usually consists of empty spaces and large surface area which thrust them to be utilized as potential candidates for diverse applications like catalysis, adsorption, sensing, gas storage, drug delivery etc.[13]

3. Synthesis of MOFs

Similar to the preparation of conventional materials, MOFs can be synthesized through different methods which are summarized in Fig. 2. Solvothermal and hydrothermal methods are most common synthesis method employed. In here the reactants and solvents (water in case of hydrothermal) are added in a closed vessel under certain temperature and pressure to yield MOFs with high degree

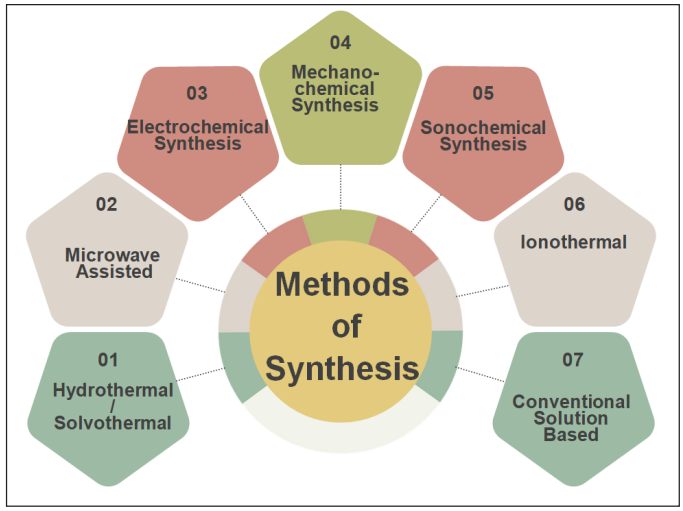

Fig. 2. *Synthetic strategies available for preparing MOFs*

of crystallinity.[14] In case of microwave synthesis, the electromagnetic waves interact with the reactants to impart high energy to the molecules resulting in fast collision and rapid uniform heating leading to formation of MOF in a brisk amount of time.[15] Electrochemical methods employ chemistry at electrode surface using electrolytic principles. Two methods namely cathodic and anodic synthesis are done and the former is more commonly used in comparison to latter. The production of MOF can be carried out continuously using this method.[16] Other methods like mechanochemical and sonochemical utilizes grinding and ultrasonic energy respectively. However the formation of undesired byproducts/low purity of target is still a major concern for both the methods.[17]

4. Stability of MOFs

Metal ions and linkers are connected through coordinative bonds which are less stable compared to covalent bonds which make them amenable to degradation in highly acidic and basic conditions. However, the linkers and metal nodes can be suitably chosen to remain stable in pH varying from 2-11. The stability of any material can be optimized by following the principles of HSAB theory which states that the combination of hard acid and hard base or soft acid and soft base result into stronger coordination compared to when they are mixed.[18] Thus, when hard acids like Al^{3+}, Cr^{3+}, Zr^{4+}, Th^{4+} etc. are combined with hard bases like $O^{2-}$from carboxylate linkers, the synthesized MOFs possess high stability under flexible pH conditions. Similarly, lower valent metal ions like Cu^{2+}, Zn^{2+}, Ni^{2+} etc. form stronger bond with nitrogen based soft linkers and remain stable. Carboxylate based MOFs are more stable in acidic conditions compared to basic because of high pK_a of linkers and vice versa for nitrogen-based linkers. The tendency of metal ions to get hydrolyze and

precipitate increase as the pH is increased and hence most of the reports generally deals with the utilization of MOFs in pH < 10.[19] Some of the water stable MOFs such as UiO-66, MIL-101, MOF-808 etc. were utilized widely for the adsorption of heavy metal ions from aqueous solutions.[20] For instance, UiO-66 is made up of tetravalent metal ions (Zr^{4+}, Ce^{4+}, Th^{4+} etc.) and dicarboxylic acid as the linker to self-assemble as a face centered cubic structure having hexanuclear cluster $[M_6O_4(OH)_4]^{12+}$ which is further attached to 6 benzene dicarboxylic acids/linkers to form a *fcu* topology with well-defined pores which can play a vital role in adsorption of different metal ions. Simpler structural representation of UiO-66 is shown as Fig. 3.

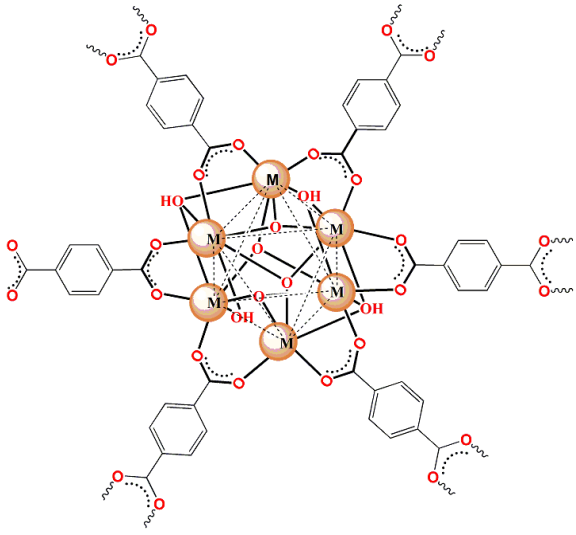

Fig. 3. Representative structure of UiO-66 showing the hexanuclear cluster; (M= Tetravalent metal ions like Zr^{4+}, Ce^{4+}, Th^{4+} etc.)

5.1 Adaptation of MOF for metal ion removal

MOFs can either be utilized as such or can be modified to form a library of materials which have suitable characteristic for the adsorption of metal ions. The most significant changes include formation of a defective structure, functionalization of MOF, formation of composite material etc.

5.1 Defective Structure

Defects in MOF structure are generally introduced through the use of simultaneous addition of an organic linker and modulator which competes for metal ion node during formation of framework. Using this strategy the surface area and pore volume is enhanced which leads to the availability of active sites benefitting the adsorption characteristic of the material.[21] Wang *et al.* reported the synthesis of defective hierarchical porous Zr based UiO-66 MOFs using dodecanoic acid as the modulator.[22]

An astonishing experimental adsorption capacity 1217 mg/g towards U (VI) was observed. Similarly, Guo *etal.* synthesized a thiol defective MOF using thio acetic acid as modulator which resulted into high –SH binding sites even after a defective structure and obtained an adsorption capacity of ~714.8 mgg^{-1} towards Hg^{2+} ion.[23]

5.2 MOF functionalization

To induce selectivity for a particular metal ion, the functionalization of either organic linker or metal node can be carried out with the former being more commonly used practice. Two strategies are employed to functionalize the MOF. In first, the linker with predefined functional groups are already present and reacted with metal ion to form a desired product. In another case, some MOFs are exceedingly stable such that the functionalization can be carried after synthesis of MOF and is not usually obtained through direct synthesis. Zhong *et al.* synthesized MOF-808 (Zr) and post-modified separately with oxalic acid and thioglycolic acid to yield MOFs with hard and soft bases respectively. MOF-808 ox could adsorb hard acids whereas MOF-TGA could efficiently adsorb soft metal ions sparing hard ions as shown in Fig. 4.[24]

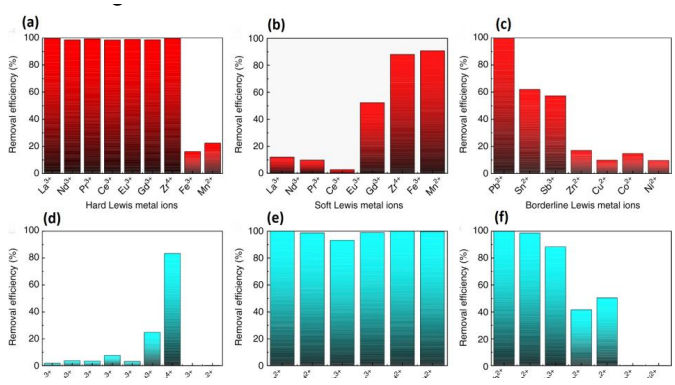

Fig. 4. Removal efficiency of heavy metal ion in single-component systems. The removal efficiency of hard Lewis metal ions, soft Lewis metal ions, and borderline Lewis metal ions for a–c MOF-808-OX, and d–f MOF-808-TGA (Reproduced from ref. [24]

5.3 MOF Composites

Combination of MOFs and other material to form a composite material having better adsorption properties than individual counterparts have been studied in detail.[25]

The improvement is attributed to the presence of synergistic effect between both the components. Different materials like graphene, activated carbon, metal oxides, magnetic nanoparticles etc. are widely used for the formation of composites. For e.g. the presence of magnetic nanoparticles like Fe_3O_4 in the matrix can aid in the separability of MOF using an external magnet. Similarly

our group devised an one step hydrothermal method to synthesize a composite of CeO_2 and UiO-66 (Ce) resulting in 25 % increase in adsorption capacity towards U (VI) compared to virgin MOF with maximum adsorption capacity of 239 mg/g as shown in Fig.5.[26]

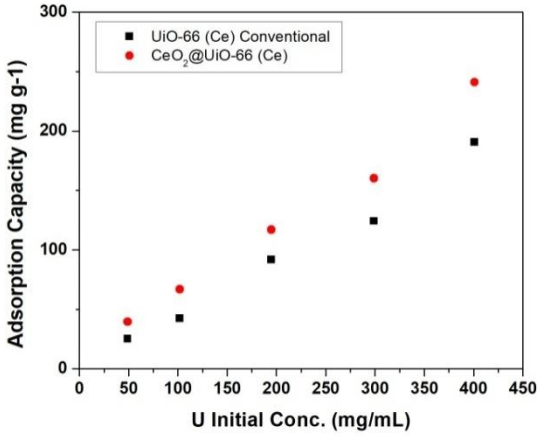

Fig. 5. Variation of adsorption capacity of UiO-66 (Ce) and CeO_2@ UiO-66(Ce) with change in initial uranium concentration

6. Factors Affecting Adsorption Performance

The adsorption characteristic of a MOF based material is evaluated through different studies which includes pH variation, adsorption kinetics, adsorption isotherm, reusability, selectivity, temperature dependent adsorption etc. Brief details for all the above-mentioned techniques are described below.

6.1 pH variation

pH can affect both the surface charge of adsorbent and the specification of metal ion.[27] In general, at lower pH MOFs are usually protonated and hence exhibit positive surface charge. As pH is increased, the deprotonation occurs and after certain pH adsorbent exhibits negative charge. The surface charge on an adsorbent can be calculated through zeta potential measurements. On the other hand, as the pH is increased different metal ions tend to hydrolyze resulting in multinuclear/hydroxide complexes and subsequently precipitating at higher pH. If electrostatic interaction is the sole factor affecting adsorption, the same can be confirmed through zeta potential measurements and correlating the metal ion species present at that pH. For instance in case of arsenate ion, the predominant species at pH 2-3 is H_3AsO_4 and maximum adsorption capacity using UiO-66 (Zr) was observed at the mentioned pH.[28] This was attributed to the fact that μ_3-OH, are responsible for binding four equivalent arsenate species with the simultaneous liberation of H^+ from H_3AsO_4 and hence proves that not only zeta potential but other factors also affect the pH dependent adsorption.

6.2 Adsorption Kinetics

The rate of adsorption of metal ion over the surface of MOF is a vital parameter of consideration since it is directly linked with the amount of power consumption. Additionally, the adsorption mechanism can be governed by rate of adsorption of metal ion. The rate of adsorption on any surface is governed by four steps.[29] The first one constitutes the transport of metal ion in the bulk of solution. The second step involves the diffusion of metal ion in close proximity of adsorbent. Third and fourth step constitutes the diffusion of metal ion in the pores of material and the binding of metal ion on the surface of adsorbate respectively. First step can generally be ignored when mixing is carried out using mechanical systems and thus not considered as rate determining step. Any of the steps could be limiting or a combination of them could also be possible. Different kinetic models are utilized to elucidate the rate determining step which mainly includes pseudo first order ((PFO) (1)), pseudo second order (PSO(2)) and Webber Morris models (3) and the corresponding equations are mentioned below.[30]

Where q_e and q_t represents adsorption capacity at equilibrium and at time '*t*' respectively. k_1, k_2 and k_i are respective rate corresponding to PFO, PSO and Weber Morris models and are dependent on operating conditions.

PFO is more commonly suited to systems in which rate limiting step is diffusion controlled. PSO is suited for those in which chemisorption is the main mode of adsorption. In Webber Morris q_t vs and if it passes through origin then intraparticle is the sole mechanism otherwise other steps are also involved. The least square fitting is carried out to know the better fit among the models described above. For more detailed understanding, reader is suggested to go through reviews already present in the literature.[31]

6.3 Adsorption Isotherm

Adsorption isotherm reveals the change in adsorption capacity as the initial concentration of heavy metal ion is increased. Adsorption isotherm is used to understand the relation between adsorbent and adsorbate under equilibrium conditions. Additionally, it can also predict accurately the maximum adsorption capacity and strength for a given system. The parameters are highly important for designing adsorption system in industrial scale. Most common models used includes Langmuir (4), Freundlich (5) and Temkin (6) isotherm models and the corresponding equations are described below.[32]

Where q_{max} and q_e denote the maximum adsorption capacity and adsorption capacity at equilibrium. K_f, K_l and A_T represents constants for respective models.

Similar to kinetic models, the experimental data is fitted using least square method. The Langmuir model assumes the adsorption to be directly proportional to fraction of sites available and adsorption occurs homogenously in monolayer. In contrast, Freundlich isotherm is applicable for cases where adsorption is occurring at heterogeneous sites with the formation of multilayers which is more common for multicomponent systems. In case of Temkin adsorption isotherm, the interactions between adsorbate molecules are assumed and the heat of adsorption of successive layers decreases as the surface coverage increases.

6.4 **Reusability Studies**

The practical use of an adsorbent is highly dependent on the number of cycles an adsorbent can be used without deteriorating with respect of initial adsorption capacity. Adsorption-desorption cycles are used where in first adsorption at MOF is carried out which is subsequently eluted using different eluents like dilute acids, bases or other solvents. For eg. our group reported a room temperature synthesis of UiO-66 (Ce) and utilized it for removal of As (V) and even after 3 adsorption-desorption cycles using 0.01 M HNO_3 as the eluent, 96% of the adsorption capacity was still retained whereas in contrast when CeO_2@UiO-66 (Ce) was utilized for uranium adsorption, it could only exhibit 35% of initial capacity as shown in Fig. 6 (a). This difference might be due to the different interactions between adsorbent and adsorbate in respective cases.

6.5 **Selectivity Studies**

The adsorption studies using MOFs are carried out using a stock solution comprising of a single metal ion and hence it is vital to determine whether the material would be able to eliminate particular metal ion in presence of number of elements simultaneously. Functionalization of MOF as described earlier is highly recommended for selective extraction of metal ion among others. For e.g. Wu *et al.* synthesized a amidoxime based UiO-66 MOF and it could adsorb uranium more than 95 % among different metal ions.[33] In our previous work, micro porous CAU-1-NH_2could selectivity adsorb Th in presence of U under different U/Th concentrations. Even at 1:5 Th/U, MOF showed higher selectivity for Th which is attributed to the higher ionic potential of Th (IV) compared to UO_2^{2+} as shown in Fig. 6 (b).

6.6 **Thermodynamic Studies**

Thermodynamics of adsorption are explored by varying the temperature of adsorption. By plotting Ln K_d as a function of temperature, the values corresponding to ΔH° and ΔS° can be calculated which are directly linked with the Gibbs free energy and calculated at different temperatures using

$$\Delta G° = \Delta H° - T\Delta S° \quad (7)$$

For instance, Chen *et al.* utilized a Cu (I) based MOF for removal of Cr (VI) and through temperature dependence studies revealed ΔG°, ΔH°, and ΔS° to be negative in nature.[34] Even though the randomness was decreasing during adsorption, the negative value ofΔG revealed the favorability of adsorption at particular temperature. However, as the temperature was increased from 288 to 328 K,ΔG was decreasing (more +ve) which hinted the unfavourability of adsorption at high temperature.

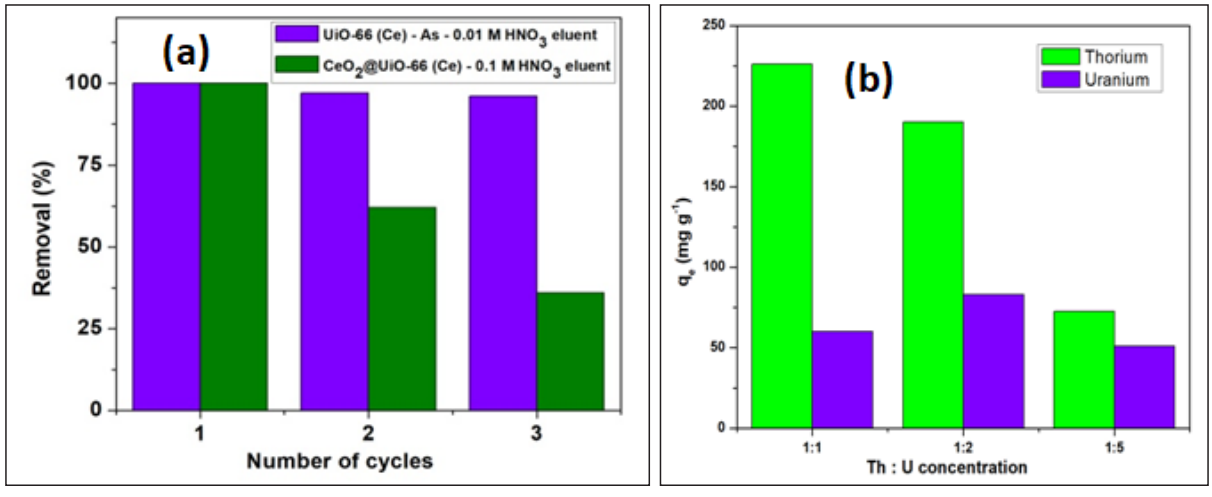

Fig. 6. (a) Th and U co-adsorbed in CAU-1 NH_2 at different Th/U ratio; (b) Effect of adsorption desorption cycles on performance of MOF

7. Decoding Adsorption Mechanism

7.1 FT-IR

After adsorption studies, it is important to understand, how the metal ion is interacting with the surface of adsorbent. To elucidate the same, different techniques namely FT-IR/Raman, XPS and theoretical modeling are generally carried out. FT-IR/Raman studies are carried to get information regarding the involvement of bond towards adsorption or the species adsorbed. For instance J. Wang *et al*. developed a MOF@COF composite and vapor adsorption of I_2 was evaluated.[35] Clear Raman signature peaks of 108 and 169 cm^{-1} corresponding to the presence of I_3^- and I_5^- were obtained which established that $I_2$was getting polarized as it came in contact with the adsorbent due to charge transfer between lone pair on N atom and σ* orbital of I_2. Similarly the adsorption of U in the form of uranyl ions (UO_2^{2+}) is confirmed by observing a peak at ~ 930 cm^{-1} in FT-IR spectrum.[36] The shift in frequency in FT-IR after adsorption is a direct consequence of involvement of particular bond towards adsorption.

7.2 X-ray Based techniques

The main feature that distinguishes XPS from FT-IR is the detection of chemical state of an element in the former technique. Since adsorption is a surface phenomenon, the changes in XPS spectrum can be easily correlated with the mechanism of adsorption. Wang *et al*. reported the adsorption and fluorescence quenching using MIL-101 NH_2 when exposed to heavy metal ions like Cu (II), Fe (III) and Pb (II).[37] The involvement of NH_2 can be easily observed through the shift of corresponding peaks in N 1s spectrum as shown in Fig. 7. Further amino groups

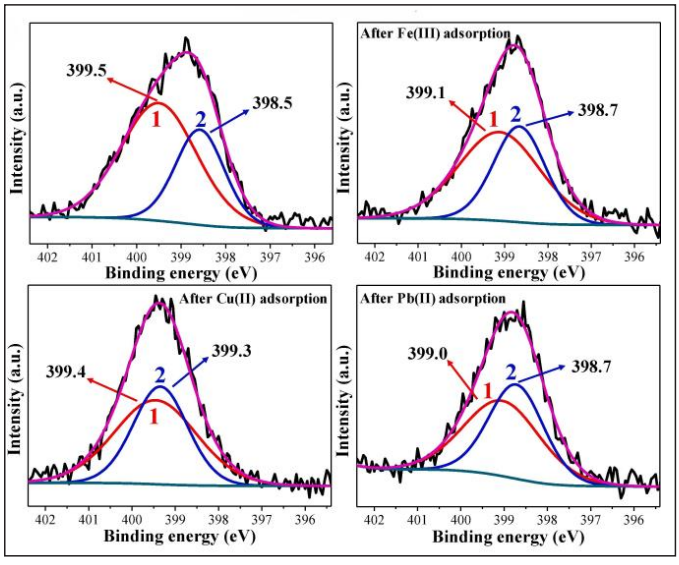

Fig. 7. XPS high-resolution spectra of N 1s for MIL-101-NH_2 before and after adsorption (Reproduced from ref. [37])

played a significant role in fluorescence turn-on or turn-off establishing the sensing property of MOF. Similarly, the involvement of –OH and –COOH in adsorption of multi heavy metal ions using MOF-808 with simultaneous coordination of Zr-O-M^{2+}occurringas observed through Zr 3d peaks as reported by Hang *et al*.[38] In addition, EXAFS is an excellent technique to predict the mode of adsorption. XPS and the near-edge X-ray absorption fine structure (NEXAFS) analysis was carried out to decipher the mechanism of adsorption revealing both N and O playing part in the chelation and with η^2 motif based model by P-UiO-66-AO based MOF.[39] EXAFS is still an underused technique as not many literature reports are available.

7.3 Computational Analysis

The mechanism predicted through abovementioned experimental techniques is generally validated through computational modeling and additional insights are also obtained.

For instance, Qian et al.[40] reported DFT studies of UiO-66 functionalized with pyro metallic acid and elucidated the Th adsorption mechanism by replacing water molecules with adsorbent groups and 3 geometries were optimized namely (i) Th(IV)@UiO-66-NH2 (ii) UiO-66-NH-PMA(–CONH) (iii) Th (IV)@UiO-66-NH-PMA1 and Th (IV)@UiO-66-NH-PMA2. The first and second model focused on interaction of Th with amino groups (as in UiO-66 NH2) and acyl amino C = O ligand + PMA respectively giving rise to distortion in latter polymer. The optimization using PMA was done through 2 models, one with ratio of 1:1 (Th^{4+}/adsorbent) and other 1:2 and the closest distance was found for the former one. Additionally, NBO analysis was done in order to predict the best model. The complex with 1:2 ratio was found to be more plausible from all the calculations observed and all the models are represented in Fig. 8. Also, modeling of entire MOF unit cell is computationally expensive and thus simpler models are usually employed. For instance we utilized CAU-1 NH_2 MOF for Th remediation and aniline moiety was considered a surrogate as the binding sites of both are analogous.[41] Geometry optimization of MOF, ligand and MOF-ligand was done as shown in Fig. 9.The positive charge on the acceptor atom of Th decreased from 1.74 in the $Th(OH)_2(H_2O)_7^{2+}$ complex to1.70 in the $Th(OH)_2(H_2O)_6$−aniline complex, suggesting an electronic charge transfer from ligand to metal during the complexation process. Also, the Wiberg bond index, which can be used to quantify the strength of the Th−N (aniline) bond in the complex, shows a value of 0.29. This indicates that a moderate interaction exists between the acceptor and donor atoms.

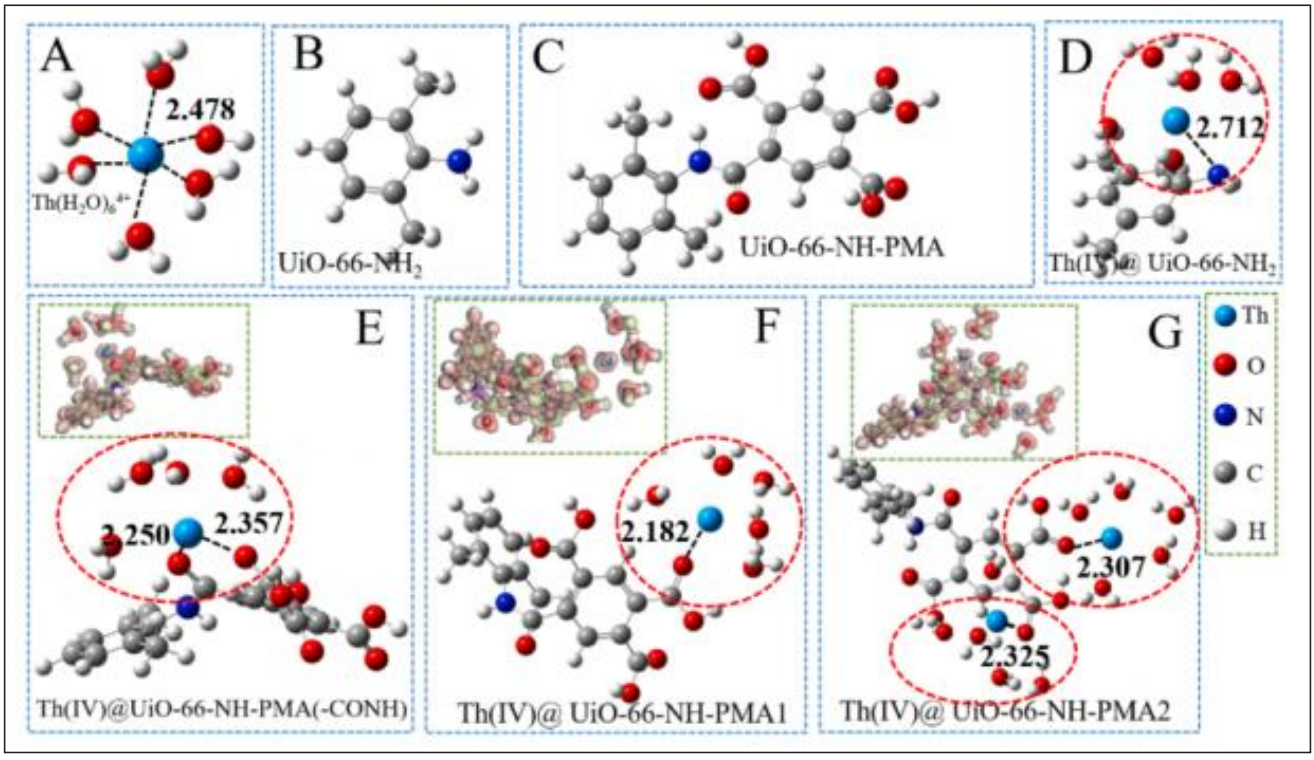

Fig. 8.The optimized configurations of (A) thorium hexahydrate $[Th(H_2O)_6]^{4+}$, (B) the simplified UiO-66-NH_2 polymer model, (C) the model of UiO-66-NH-PMA, (D) 1:1 ratio of Th(IV) adsorption on amino group, (E) 1:1 ratio of Th(IV) adsorption on C = O ligands of acylamino group and PMA, (F) 1:1 ratio of Th(IV) with C = O ligands on the PMA of UiO-66-NH-PMA chain, and (G) 1:2 ratio of Th(IV) with C = O ligands on the same UiO-66-NH-PMA chains. (Reproduced from ref. [41])

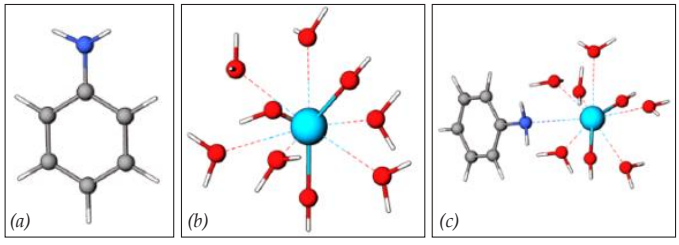

Fig. 9. Optimized geometries of the lowest energy structure for (a) aniline, (b)$Th(OH)_2(H_2O)_7^{2+}$and (c) $Th(OH)_2(H_2O)_6$-$aniline^{2+}$ at BP86/def2-TZVP level

8. Conclusion & Future Potential

In this report a brief description of MOF for the removal of heavy metal ions is described with emphasis given on synthesis methods and the factors affecting the adsorption characteristics. They are modified through formation of defective structure, ligand functionalization or composite formation depending on the heavy metal ion of interest to be removed. Even though MOFs is a hot topic among material scientists, the practical application of MOF towards nuclear waste remediation is limited which is due to the concerns regarding acid instability of MOF. In addition, the radiation satiability of MOFs is not well known and hence a lot of R&D scope is there before these can be utilized in nuclear industry.

References

1. H. Pezeshki, M. Hashemi, S. Rajabi, Heliyon, 9 (2023) e14246.
2. H.N. Muhammad Ekramul Mahmud, A.K.O. Huq, R.b. Yahya, RSC Advances, 6 (2016) 14778-14791.
3. V. Balaram, A. Rani, D.P.S. Rathore, Geosystems and Geoenvironment, 1 (2022) 100043.
4. Z.-J. Fu, S.-K. Jiang, X.-Y. Chao, C.-X. Zhang, Q. Shi, Z.-Y. Wang, M.-L. Liu, S.-P. Sun, Water Research, 222 (2022) 118888.
5. N.A.A. Qasem, R.H. Mohammed, D.U. Lawal, npj Clean Water, 4 (2021) 36.
6. M. Karnib, A. Kabbani, H. Holail, Z. Olama, Energy Procedia, 50 (2014) 113-120.
7. K. Geng, T. He, R. Liu, S. Dalapati, K.T. Tan, Z. Li, S. Tao, Y. Gong, Q. Jiang, D. Jiang, Chemical Reviews, 120 (2020) 8814-8933.
8. S. Zhang, Q. Yang, C. Wang, X. Luo, J. Kim, Z. Wang, Y. Yamauchi, Advanced Science, 5 (2018) 1801116.
9. M.S. Lohse, T. Bein, Advanced Functional Materials, 28 (2018) 1705553.
10. H. Li, M. Eddaoudi, M. O'Keeffe, O.M. Yaghi, Nature, 402 (1999) 276-279.
11. M. Eddaoudi, J. Kim, N. Rosi, D. Vodak, J. Wachter, M. O'Keeffe, O.M. Yaghi, Science, 295 (2002) 469-472.
12. V.F. Yusuf, N.I. Malek, S.K. Kailasa, ACS Omega, 7 (2022) 44507-44531.

13. D. Li, A. Yadav, H. Zhou, K. Roy, P. Thanasekaran, C. Lee, Global Challenges, 8 (2024) 2300244.
14. S.T. Meek, J.A. Greathouse, M.D. Allendorf, Advanced Materials, 23 (2011) 249-267.
15. Y.-R. Lee, J. Kim, W.-S. Ahn, Korean Journal of Chemical Engineering, 30 (2013) 1667-1680.
16. A. Martinez Joaristi, J. Juan-Alcañiz, P. Serra-Crespo, F. Kapteijn, J. Gascon, Crystal Growth & Design, 12 (2012) 3489-3498.
17. G. Lin, B. Zeng, J. Li, Z. Wang, S. Wang, T. Hu, L. Zhang, Chemical Engineering Journal, 460 (2023) 141710.
18. S. Yuan, L. Feng, K. Wang, J. Pang, M. Bosch, C. Lollar, Y. Sun, J. Qin, X. Yang, P. Zhang, Q. Wang, L. Zou, Y. Zhang, L. Zhang, Y. Fang, J. Li, H.-C. Zhou, Advanced Materials, 30 (2018) 1704303.
19. I.T.Y. Lam, S.-J. Choi, D. Lu, Y. Kim, Nanoscale, 15 (2023) 10189-10205.
20. S. Essalmi, S. Lotfi, A. BaQais, M. Saadi, M. Arab, H. Ait Ahsaine, RSC Advances, 14 (2024) 9365-9390.
21. J. Ren, M. Ledwaba, N.M. Musyoka, H.W. Langmi, M. Mathe, S. Liao, W. Pang, Coordination Chemistry Reviews, 349 (2017) 169-197.
22. C. Yin, Q. Liu, R. Chen, J. Liu, J. Yu, D. Song, J. Wang, Industrial & Engineering Chemistry Research, 58 (2019) 1159-1166.
23. X. Gao, B. Liu, X. Zhao, Chemosphere, 317 (2023) 137891.
24. Y. Peng, H. Huang, Y. Zhang, C. Kang, S. Chen, L. Song, D. Liu, C. Zhong, Nature Communications, 9 (2018) 187.
25. I. Ahmed, S.H. Jhung, Materials Today, 17 (2014) 136-146.
26. N. Gumber, R.V. Pai, K. Sanyal, B. Dutta, P.A. Hassan, Microporous and Mesoporous Materials, 341 (2022) 112108.
27. J. Li, X. Dong, X. Liu, X. Xu, W. Duan, J. Park, L. Gao, Y. Lu, Sustainability, 14 (2022) 15579.
28. C. Wang, X. Liu, J.P. Chen, K. Li, Scientific Reports, 5 (2015) 16613.
29. V. Krstić, Chapter 14 - Role of zeolite adsorbent in water treatment, in: B. Bhanvase, S. Sonawane, V. Pawade, A. Pandit (Eds.) Handbook of Nanomaterials for Wastewater Treatment, Elsevier, 2021, pp. 417-481.
30. J. Wang, X. Guo, Journal of Hazardous Materials, 390 (2020) 122156.
31. K. George William, E. Serkan, Ö. Atakan, H.K. Özcan, A. Serdar, Modelling of Adsorption Kinetic Processes—Errors, Theory and Application, in: E. Serpil (Ed.) Advanced Sorption Process Applications, IntechOpen, Rijeka, 2018, pp. Ch. 10.
32. J. Wang, X. Guo, Chemosphere, 258 (2020) 127279.
33. Q. Gao, M. Wang, J. Zhao, M. Zhang, D. Shao, J. Hu, G. Wu, Microporous and Mesoporous Materials, 329 (2022) 111511.
34. H. Qi, X. Niu, H. Wu, X. Liu, Y. Chen, Journal of Chemistry, 2021 (2021) 4413095.
35. J. Wang, L. Wang, Y. Wang, F. Yang, J. Li, X. Guan, J. Zong, F. Zhou, J. Huang, Y.-N. Liu, Chemical Engineering Journal, 438 (2022) 135555.
36. W. Wang, S. Ni, Y. Liu, Y. Zhao, Y. Meng, L. Yang, Separation and Purification Technology, 346 (2024) 127409.
37. S.-W. Lv, J.-M. Liu, C.-Y. Li, N. Zhao, Z.-H. Wang, S. Wang, Chemical Engineering Journal, 375 (2019) 122111.
38. Z. Xie, S. Diao, R. Xu, G. Wei, J. Wen, G. Hu, T. Tang, L. Jiang, X. Li, M. Li, H. Huang, Applied Surface Science, 636 (2023) 157827.
[39] L. Ma, C. Huang, Y. Yao, M. Fu, F. Han, Q. Li, M. Wu, H. Zhang, L. Xu, H. Ma, Separation and Purification Technology, 314 (2023) 123526.
[40] Q. Peng, B. Huang, L. Peng, D. Guo, T. Jin, Z. Liu, Y. Qian, Separation and Purification Technology, 337 (2024) 126391.
[41] N. Gumber, R.V. Pai, J. Bahadur, S. Sengupta, D. Das, U.K. Goutam, ACS Omega, 8 (2023) 12268-12282.

Shri Nitin Gumber is currently working as a Scientific Officer in Fuel Chemistry Division, BARC after graduating from 62nd batch of BARC Training School at IGCAR campus. He received his B.Sc. degree from Panjab University, Chandigarh and was awarded with gold medal. He did his M.Sc. from Indian Institute of Technology, Indore. After joining FCD he has been working on applications of Metal Organic Frameworks for remediation of heavy metal ions from aqueous solutions and development of different matrices for HLW immobilization. He has more than 20 publications to his name including both journal and conference articles.

Dr. Rajesh V. Pai, joined Fuel Chemistry Division in 1997 through 40th batch of Training School after completion of his MSc from Cochin University of Science and Technology. Since then he has been working on development of nuclear fuel materials by sol gel process. He obtained his PhD from Mumbai University. He has developed many flow sheets suitable for fabrication of advanced nuclear fuel materials and special fuels by sol-gel process. He is an expert in synthesizing many technologically important materials such as perovskites, pyrochlores, layered perovskites etc. which are used as peizo electric, catalytic, chemical sensors in different applications. He has published about 45 papers in international journals, 3 book chapters and one monograph. His current interest includes the development and functional studies of various advanced porous materials like Metal-organic Frameworks (MOFs) and composite materials. Currently he is a Professor at HBNI, DAE and Head, Fuel Chemistry Division, BARC.

Influence of Dithioglycol on Iodine Adsorption Properties of HKUST-1

S. Kolay
Chemistry Division, Bhabha Atomic Research Centre, Mumbai-400085, India
Email: siddhart@barc.gov.in

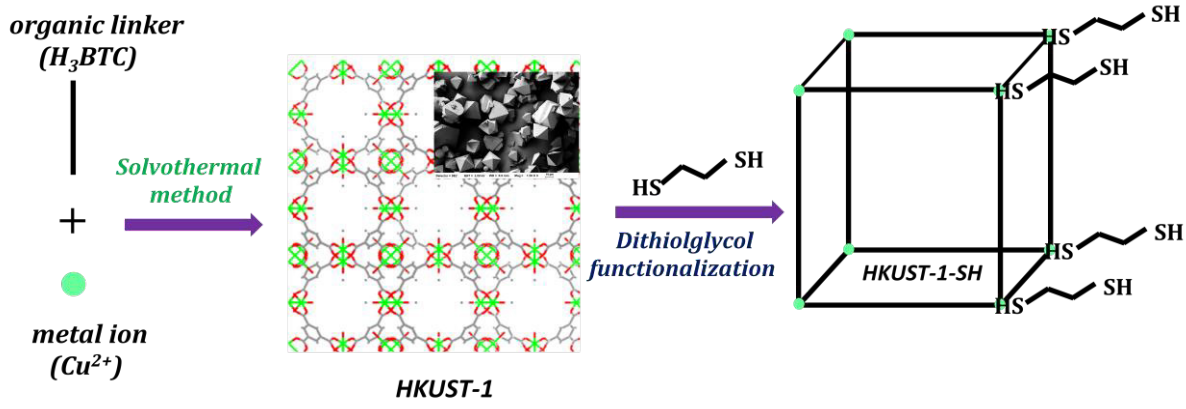

Graphical abstract

1. Introduction

Limited resources and adverse environmental effect of traditional fossil fuel encourage the scientific community to look for alternate energy source to meet the growing energy demand. Nuclear being high density green energy finds prominent attention as alternate to the traditional fossil fuel [1]. Currently, ~10% of the world's total electricity is being contributed by nuclear energy with promising growth trend [2,3]. However, the radioactive nuclear wastes generated during nuclear fission poses a serious concern to the environment and needs to be sequestrated from the off gas mixture before gets released to the environment. Among the volatile radio-nuclides, radioactive iodine, especially ^{129}I poses serious concern because of its long half life ($t_{1/2}$ 1.57×10^{7} yrs), easy diffusion through air/water and active participation in bio-metabolism [4-6]. Therefore, a reliable and trustworthy approach must be implemented for efficient capture and storage of radioactive iodine [7, 8].

During last decades, various materials and methods have been developed for iodine capture. Out of them, adsorption through solid adsorbent is considered as the most realistic and convenient one. Activated carbon, TEDA-impregnated activated carbon, silver impregnated zeolite, mordenite, etc, are some of the much studied solid adsorbent [9-16]. However, low adsorption capacity, limited chemical & thermal stability, difficult to functionalization, poor recyclability and high cost of silver limit their real life application.

Over recent years, a new class of crystalline porous materials, known as metal organic frameworks (MOFs) have established their potential as alternate solid adsorbent. High specific surface area, tuneable porosity, optimum chemical & thermal stability and easy functionalization are some of the major advantages of MOFs over conventional adsorbents and hence attract the scientific community to explore them as alternate adsorbent for iodine [17-26]. Iodine adsorption by MOFs has been reported by many groups [19-22, 27-34]. Here, we have explored the effect on dithioglycol functionalization of HKUST-1 on its iodine adsorption characteristics.

2.0 Experimental Section

2.1 Materials and methods

All chemicals and solvents (except toluene) used during experiments are of commercially available and were used without any further purification. Toluene was dried over sodium following standard procedure.

2.2 Characterizations

Powder X-ray diffractions (PXRD) were recorded using SmartLab powder X-ray diffractometer (Rigaku, Japan) with Ni filtered Cu-Kα radiation. Fourier transform infrared spectra (FTIR) were recorded using Alpha-II spectrophotometer (Bruker make) in attenuated total reflection (ATR) mode in the wavenumber region 400 to 4000 cm^{-1}. Raman spectra were recorded using Horiba JobinYvon Raman Spectrometer (model: LabRAM

HR800, λ: 632.8 nm using He-Ne laser at 17 mW power). BET surface areas were calculated from N_2 adsorption-desorption isotherms measured at 77 K using AutosorbiQ Station 2 instrument. TG were recorded using Setsys Evolution 1750, SETARAM, France with a heating rate of 5 °C/min under argon flow. SEM was recorded using field emission gun-scanning electron microscope (FEG-SEM), (make: ZEISS, model: AURIGA)

2.3 Adsorption-desorption studies

Activated sample (50 mg) was taken in a 10 mL beaker and placed inside a seal chamber. 0.5 g crystalline I_2 was taken in another 10 mL beaker and placed inside the same chamber as shown in **Fig. 1**. The whole chamber was kept at 80 °C. After a pre-defined time period, the sample was taken out from the seal chamber and kept at 80 °C for 2 minutes to get rid of surface adsorbed iodine, cooled in desiccator and weighed. I_2uptake, Q (g/g) was calculated gravimetrically based on equation 1.

$$Q = \frac{w_2 - w_1}{w_1} \quad \text{----------} \quad (1)$$

w_1 and w_2 are the weight of the sample before and after iodine adsorption.

Iodine desorption from the host matrix was carried out by two ways: heating at 150 °C for 12 hours in air or by washing with ethanol at room temperature.

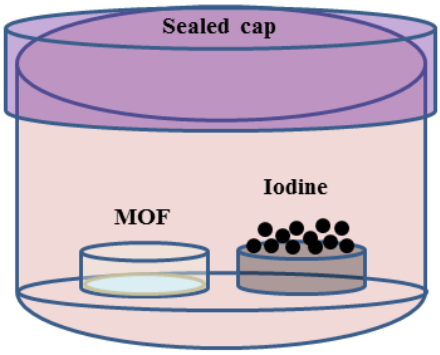

Fig. 1. Experimental set up for I_2 adsorption studies at 80 °C.

2.4 Synthesis of $[Cu_3(BTC)_2(H_2O)_3]_n$ (HKUST-1)

Highly crystalline $[Cu_3(BTC)_2(H_2O)_3]_n$ (HKUST-1) have been synthesized based on solvothermal technique. Typically, $Cu(NO_3)_2.3H_2O$ (3.0 g, 12.4 mmol) was dissolved in 150 mL 1:1 (v/v) water-ethanol mixture under stirring. H_3BTC (1.2 g, 5.7 mmol) was added to the above solution and magnetically stirred for additional 30 minutes. The mixture was transfer to a Teflon-lined stainless steel autoclave and heated at 120 °C for 12 hours. Blue colour highly crystalline powder was collected by filtration, washed repeatedly with water, ethanol and finally activated at 150 °C.

2.5 Synthesis of dithioglycol functionalized $[Cu_3(BTC)_2]_n$(HKUST-1-SH)

Dithioglycol functionalized $[Cu_3(BTC)_2]_n$, denoted as HKUST-1-SH was synthesized using phase inversion technique. Typically, 2.0 g of activated HKUST-1 was dispersed in 15 mL dry toluene. Respective amount of dithioglycol (ρ = 1.12 g/mL) (0.20 mL for sample-I and 0.47 mL for sample-II) was diluted with 2 mL dry toluene and added drop wise under stirring. After overnight stirring at room temperature, the powder was collected by filtration, washed with ethanol and dried at room temperature. Finally, the powder was activated by heating at 80 °C under vacuum for 24 hours.

3.0 Results and discussion

3.1 Characterization of HKUST-1 and HKUST-1-SH

Reaction of $Cu(NO_3)_2.3H_2O$ with H_3BTCin water-ethanol mixture under solvothermal condition yielded blue colour highly crystalline $[Cu_3(BTC)_2(H_2O)_3]_n$ (HKUST-1). X-ray diffraction pattern of the synthesized powder along with SEM micrograph and simulated XRD pattern generated from single crystal XRD data are shown in Fig. 2. Excellent agreement between synthesized and simulated pattern signifies the formation and purity of the framework. Uniform micron size octahedrons with sharp edges are clearly visible from the SEM micrograph. Since the loosely bound axially coordinated water molecules in $[Cu_3(BTC)_2(H_2O)_3]_n$ can be easily de-coordinated by heating at 150 °C resulting unsaturated metal centre, HKUST-1 can be considered as an excellent matrix for selective functionalization using post synthetic modification technique (PSM). Keeping that in mind, in the present work, the unsaturated copper centres in $[Cu_3(BTC)_2]_n$ has been successfully functionalized with dithioglycol following a reported procedure [27]. PXRD patterns of the functionalized samples (**Fig. 2)** can be easily indexed based on HKUST-1's pattern and hence confirm the retention of three dimensional (3D) structure even after PSM. However, overall diffraction peak intensities decreases upon dithioglycol functionalization. The decrease in intensity is more in sample-II compare to sample-I and is in accordance with dithioglycol concentration.

TG analyses (**Fig. 2(iv)**) also confirm the presence of dithioglycol in the PSM samples as indicated from their corresponding weight loss steps. Different sample shows different weight loss profiles. Weight loss in the

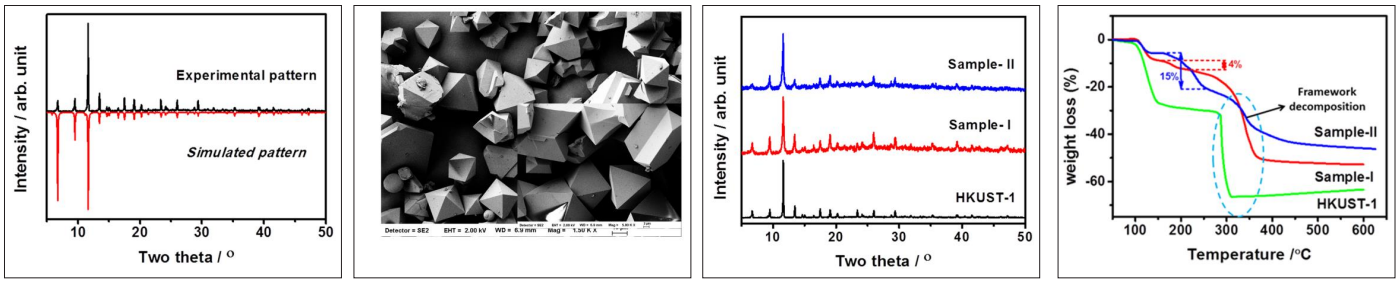

Fig. 2 **(i)** *PXRD patterns of the synthesized and simulated HKUST-1;* **(ii)** *FESEM images of Synthesized HKUST-1;* **(iii)** *PXRD patterns after dithioglycol functionalization; (iv) TGA profiles of HKUST-1 and HKUST-1-SH samples, recorded under flowing Argon with heating rate 5 °C/minute.*

temperature range 95 – 155 °C is due to water coordinated to copper centre and the proportion gradually decrease from HKUST-1 to sample-I to sample-II, attributing its substitution by dithioglycol. Weight loss in the temperature range 160 – 260 °C is due to dithioglycol and is more (15 %) in case of sample-II compare to sample-I (4 %) indicating higher extent of functionalization in sample-II than sample-I. Structural breakdown and framework decomposition takes place at 280 – 380 °C with sharp weight loss. FTIR Spectra (**Fig. 3**) of HKUST-1 matches well with the spectra reported by P. Musto et. al [28]. Peaks at 728 and 752 cm^{-1} are due to Cu centre chelation with O-C=O groups. Aromatic ring stretching vibration appears at 1372 cm^{-1}. Bands around 1630 and 1445 cm^{-1} are due to asymmetric and symmetric stretching vibration of –O-C-O- group. Peak at 480 cm^{-1} is due to Cu-O stretching vibration. FTIR spectra of dithioglycol functionalized samples (sample-I & II) are identical to the spectra reported by F. Ke and his group [29]. Presence of dithioglycol is indicated from the absorption bands at 682 and 2560 cm^{-1} corresponding to ν(C-S) and ν(S-H), respectively. Gradual increase of relative band intensities characteristic to dithioglycol from sample-I to sample-II also reflect the presence of higher concentration of dithioglycol in sample-II than sample-I and hence higher extent of functionalization in sample-II than sample-I.

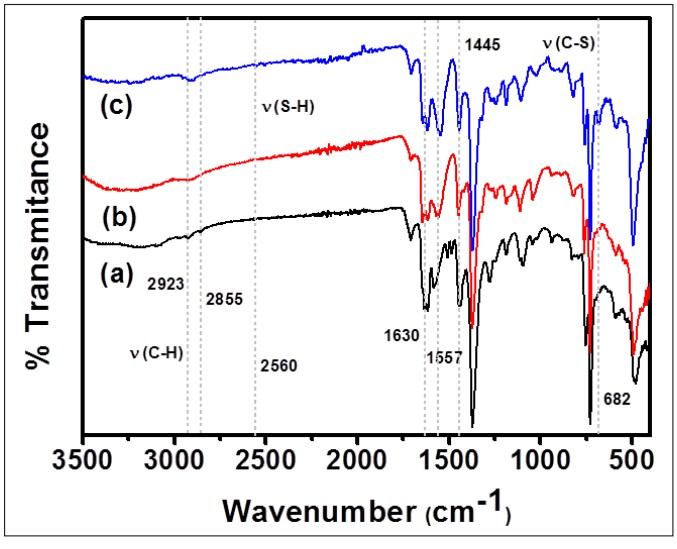

Fig. 3. **(i)** *FTIR spectra of:* **(a)** *$[Cu_3(BTC)_2(H_2O)_3]_n$ (HKUST-1);* **(b)** *HKUST-1-SH (sample-I) and* **(c)** *HKUST-1-SH (sample-II).*

3.2 BET measurement

Porous nature of the powders were find out from N_2 adsorption-desorption isotherms measured at 77 K. Isotherms are shown in **Fig. 4** and the corresponding characteristic porosity parameters are tabulated in **Table-1**. HKUST-1 shows a specific surface area of 946 m^2/g and is in good agreement with the reported value [30]. Considerable modifications in isotherm nature are observed after PSM with decrease in surface area. Such decrease in surface area and pore volume upon PSM suggests partial occupation of some of the inner pore space with dithioglycol.

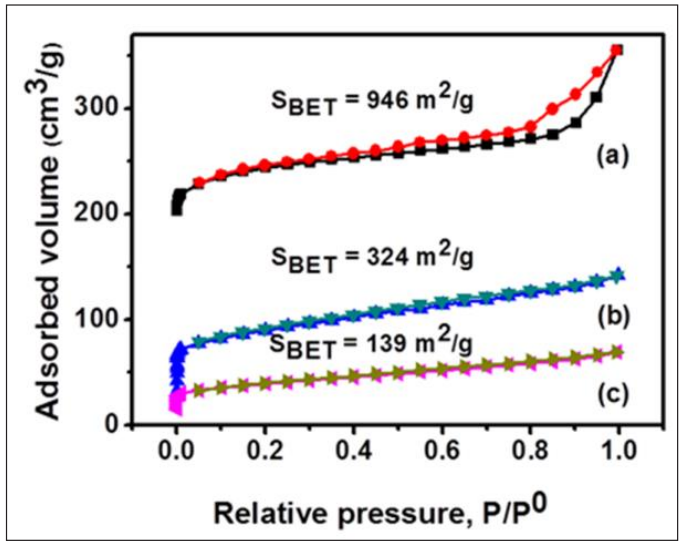

Fig. 4 N_2 adsorption-desorption isotherms at 77 K of **(i):** **(a)** *HKUST-1;* **(b)** *HKUST-1-SH (sample-I) &* **(c)** *HKUST-1-SH (sample-II).*

Table 1 Characteristic porosity parameters.

Sample	S_{BET} (m^2/g)	V_t (cc/g)	D_{Pore} (nm)
HKUST-1	946.07	0.55	2.33
HKUST-1-SH (*sample-I*)	324.40	0.22	2.71
HKUST-1-SH (*sample-II*)	139.10	0.11	3.09

3.3 Adsorption - desorption studies

In order to evaluate the effect of dithioglycol functionalization on I_2 adsorption characteristics of HKUST-1, time dependent I_2 adsorption performance of HKUST-1, HKUST-1-SH (sample-I & II) has been evaluated at 80 °C through vapour diffusion technique. Detail procedures are mentioned in experimental section. Typically, I_2 adsorption was measured gravimetrically after exposing the sample to excess I_2 vapour in a seal container for a pre-defined duration. **Figure 5** shows the time dependent I_2 uptake by the powder samples and fittings with respect to pseudo first order, pseudo second order and particle diffusion kinetic models. I_2 adsorption by much studied HKUST-1 has been previously reported by many groups [21, 31]. In the present study also, I_2 adsorption by HKUST-1 has been carried out and shown in **Fig. 5**. Upon dithioglycol functionalization, there observed a profound improvement in the adsorption characteristics. Unlike HKUST-1, I_2 adsorption by HKUST-1-SH (Fig. 5(i)) takes place through two well separated steps: an initial fast adsorption followed by a comparatively sluggish adsorption. Sample-II having higher dithioglycol concentration shows superior saturation capacity than sample-I. Sample-I can adsorb 0.6 g/g of I_2 in the first step within 2 hours and altogether 0.9 g/g within 20 hours before reaching the saturation. Sample-II can adsorb 1.0 g/g I_2 in the first step within 4 hours and altogether 1.8 g/g within 18 hours before reaching the saturation.

To explore the adsorption mechanism, kinetic data were fitted with three different adsorption kinetic models, namely, pseudo-first order, pseudo-second order and particle diffusion models (**Fig. 5**). It can be seen from the fitted plots that the data can be better fitted with pseudo-

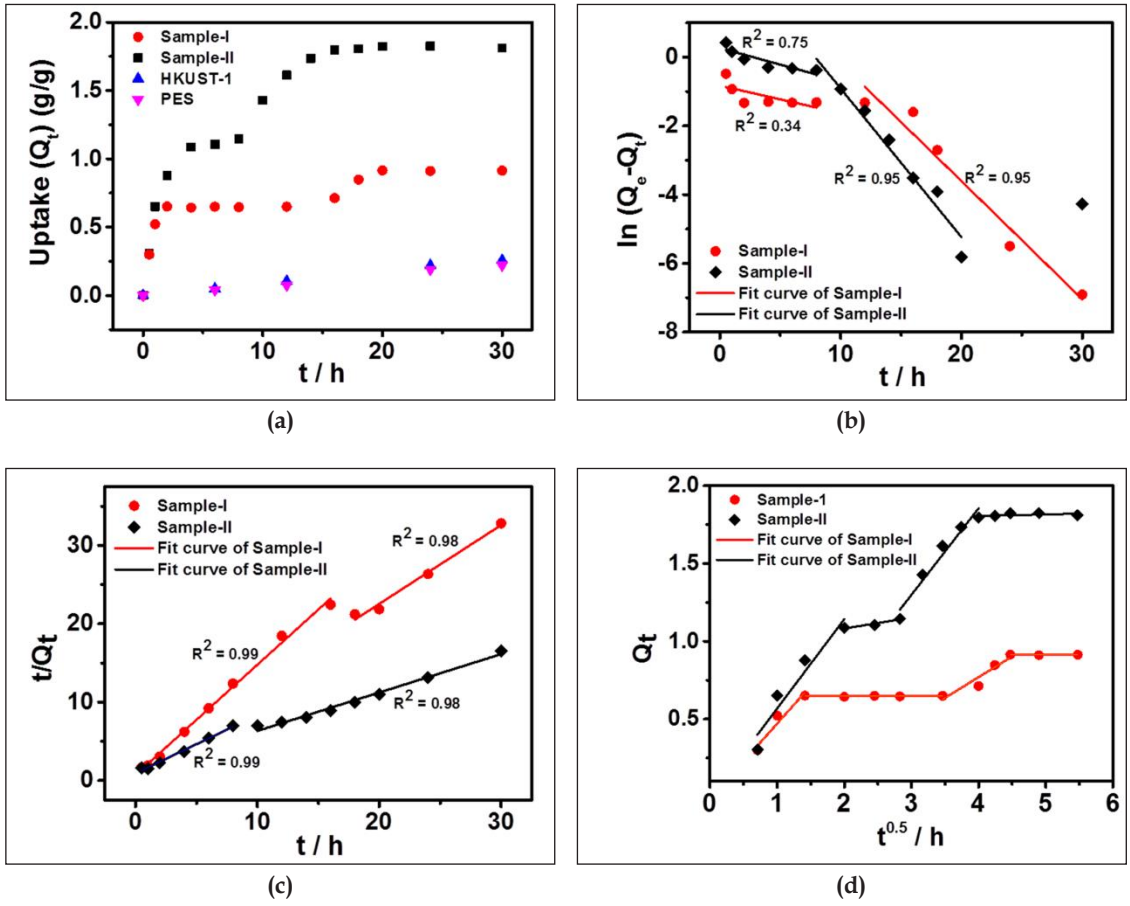

Fig. 5(**a**) *Time dependent gravimetric I_2 adsorption characteristics by powder samples at 80°C;* (**b**) *Pseudo first order kinetics model fitting;* (**c**) *Pseudo second order kinetics Model fitting;* (**d**) *Particle diffusion model fitting.*

second order model than pseudo-first order (considering correlation coefficient, R^2) indicating the presence of both physical and chemical interactions during the adsorption process. Presence of multi-linear portions in uptake (Q_t) vs time $^{1/2}$ plots for both powders as well as composite beads indicate the involvement of more than one steps in the adsorption process [32].

Desorption of iodine from the host matrix has been carried out using both thermal as well as soft chemical methods. TG plots of sample-II after different percentages of I_2 adsorption are shown in **Fig. 6**. In line with the above second order kinetic model, thermal desorption of iodine takes place at two temperatures. Desorption at low temperature (~150 °C) is due to physically bound iodine and the desorption after 400 °C is due to chemically bound iodine. Physically bound iodine can also be desorbed by washing with ethanol at room temperature.

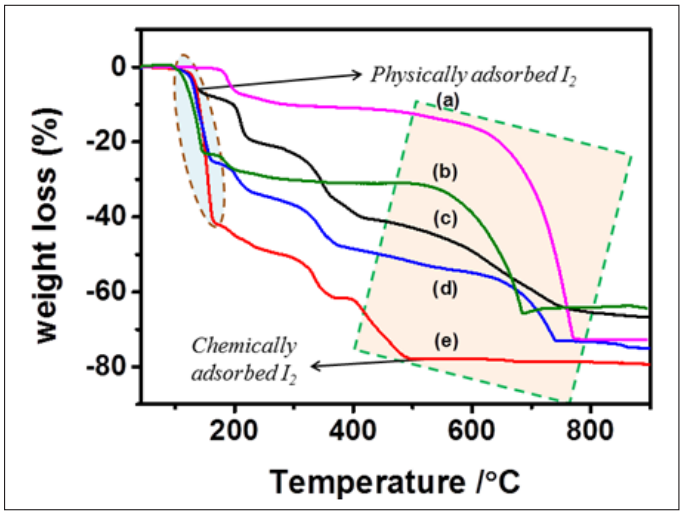

Fig. 6. TG plots of: (**a**) *CuI($C_2S_2H_6$)$_{0.25}$ obtained after washing I_2 adsorbed sample-II with ethanol;* (**b**) *CuI($C_2S_2H_6$)$_{0.25}$ after I_2 adsorption;* (**c**) *sample-II@I_2 (I_2adsorbed: 36 wt%);* (**d**) *sample-II@I_2 (I_2adsorbed: 110 wt%) and* (**e**) *sample-II@I_2 (I_2adsorbed: 179 wt%). Heatingrate:5 °C/ min under flowing argon.*

3.4 XRD and Raman spectroscopic studies

XRD, Raman and X-ray photoelectron spectroscopic (XPS) studies has been carried out to elucidate the nature of interaction between iodine and the host matrix. Contrary to HKUST-1 where iodine adsorption takes place through intra-molecular hydrogen bonding interactions [21], in dithioglycol functionalized HKUST-1, iodine adsorption takes place following a completely different pathway. **Fig. 7 (i)** represents the XRD patterns of sample-II after various amount of iodine adsorption. Thus, upon iodine adsorption, characteristic diffraction peaks due to HKUST-1-SH disappear with the formation of some strong peaks attributed to γ-CuI (ICSD No. 33726). Though, at lower concentration of adsorbed iodine, diffraction peaks corresponding to γ-CuI are only seen, at higher concentration of adsorbed iodine, additional set of peaks are also seen with gradual increase in peak intensities with adsorbed iodine concentrations. Therefore, structural breakdown of the framework takes place during adsorption due to strong interaction between copper and iodine. In the subsequent step, CuI acts as secondary adsorbent and converted into CuI@I_2 through molecular iodine adsorption. In Raman studies (Fig. 7(ii)), five peaks (109, 124, 162, 181 & 210 cm^{-1}) are observed and the relative peak intensities changes depending upon adsorbed iodine concentrations. These peaks can be divided into two sub-group characteristic of two steps in adsorption vs time plot (**Fig. 5(a)**). In all cases, peaks at 109, 124 & 162 cm^{-1} are seen. Peaks at 124 cm^{-1} are due to CuI [33]. Peaks at 109 & 162 cm^{-1} can be assigned as due to I_3^- and / or I_5^-, respectively [54, 55]. Formation of I_5^- might have taken place through [(trimesic acid)$_{10}$H]I_5 formation as was reported by B. Orel et. al [34] through framework decomposition and CuI formation. With further adsorption of iodine (> 64 wt% for sample-I & > 110 wt% for sample-II), two additional peaks at 181 & 210 cm^{-1} characteristic of molecular iodine can be seen. It is clearly visible from the spectra that the relative peak intensities corresponding to molecular iodine increases with increase in adsorbed iodine concentrations which signifies the adsorption of more and more molecular iodine in the second step of uptake vs time plots (**Fig. 5**).

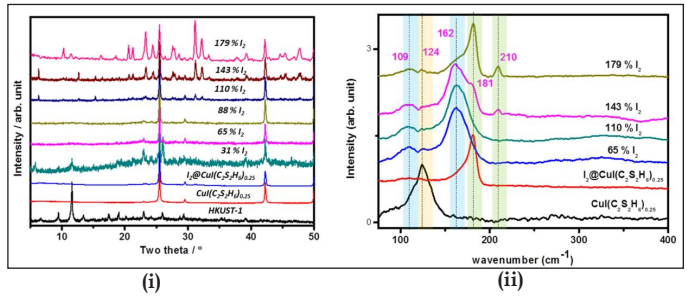

Fig. 7(**i**) *PXRD patterns of sample-II after different weight % of I_2 adsorption;* (**ii**) *Raman spectra of sample-II after different weight % of I_2 adsorption.*

4. Conclusion

In summary, here we have synthesized dithioglycol functionalized HKUST-1 and evaluated its iodine adsorption performance at 80 °C. The framework shows improve adsorption characteristics compare to pristine HKUST-1 with much fast kinetics. Employing PXRD, TG and Raman spectroscopy, the nature of host-guest interaction taking place during the adsorption process has been established. It has been observed that unlike HKUST-1 where iodine adsorption is taking place through intra-

molecular hydrogen bonding interactions, the adsorption in dithioglycol functionalized HKUST-1 is taking place through both physisorption and chemisorption means. During iodine adsorption, transformation of HKUST-1-SH to γ-CuI and γ-CuI into γ-CuI@I_2 is clearly evidenced from Raman studies.

References

1. Nuclear energy in a sustainable development perspective, OECD Nuclear Energy Agency, 2000.
2. WNA, IAEA, Nuclear Engineering International, June 2014, http://worldnuclear.org/information-library/current-and-future-generation/nuclear- power-in-theworld-today.aspx.
3. IAEA Annual Report 2012, http://nei.org/News-Media/News/News- Archives/IAEAProjects-up-to-100-Growth-of-Nuclear-Energy-b.
4. F. C. Küpper, M. C. Feiters, B. Olofsson, T. Kaiho, S. Yanagida, M. B. Zimmermann,L. J. Carpenter, G. W. Luther III, Z. Lu, M. Jonsson and L. Kloo, *Angew. Chem. Int. Ed.*, 2011, **50**, 11598.
5. A. Saiz-Lopez, J. M. C. Plane, A. R. Baker, L. J. Carpenter, R. von Glasow, J. C. Gómez Martin, G. McFiggans and R. W. Saunders,*Chem. Rev.*, 2012, **112**, 1773.
6. M. I. Ojovan and W.E. Lee, An Introduction to Nuclear Waste Immobilisation (Second Edition), 2014.
7. D. Haefner, Methods of Gas Phase Capture of Iodine from Fuel Reprocessing Off Gas: A Literature Survey (Technical Report), 2017.
8. B.J. Riley, J. Chun, J.V. Ryan, J. Matyáš, X.S. Li, D.W. Matson, S. K. Sundaram, D. M. Strachan and J. D. Vienna, *RSC Adv.*,**1**, 2011, 1704.
9. K. W. Chapman, P. J. Chupas and T. M. Nenoff, *J. Am. Chem. Soc.*,2010, **132**, 8897.
10. T. M. Nenoff, M. A. Rodriguez, N. R. Soelberg and K. W. Chapman,Micropor. Mesopor. Mat.,2014, **200**,297.
11. S. W. Park, H. S. Park, W. K. Lee and H. Moon, *Separ. Technol.*,1995, **5**, 35.
12. C. M. González-García, J. F. González and S. Román, *Fuel Process.Technol.*, 2011,**92**, 247.
13. R. Jubin, report No. CONF-811108-14 (Oak Ridge National Laboratory, 1981).
14. K. Funabashi, T. Fukasawa and M. Kikuchi,*Nucl. Technol.*,1995, **109**, 366.
15. R. D. Scheele, L. L. Burger and C. L. Matsuzaki, *Report No. PNL-4489* (Pacific National Lab, 1983).
16. S. Nandanwar, K. Coldsnow, V. Utgikar, PiyushSabharwall and D. Eric Aston, *J. Chem. Eng.*, 2016, **306**, 369.
17. G. Férey, *Chem. Soc. Rev.*, 2008, **37**,191.
18. S. M. Cohen, *Chem. Rev.*, 2012, **112**, 970.
19. C. Falaise, C. Volkringer, J. Facqueur, T. Bousquet, L. Gasnot and T. Loiseau, *Chem. Commun.*, 2013, **49**, 10320.
20. D. F. Sava, M. A. Rodriguez, K. W. Chapman, P. J. Chupas, J. A. Greathouse, P. S. Crozier and T. M. Nenoff, *J. Am. Chem. Soc.*, 2011, **133**, 12398.
21. D. F. Sava, K. W. Chapman, M. A. Rodriguez, J. A. Greathouse, P. S. Crozier, H. Zhao, P. J. Chupas and T. M. Nenoff, Chem. Mater., 2013, **25**, 2591.
22. K.W. Chapman, D.F. Sava, G.J. Halder, P.J. Chupas, T.M. Nenoff, *J. Am. Chem. Soc.*, 2011, **133**, 18583.
23. P. Mao, B. Qi, Y. Liu, L. Zhao, Y. Jiao, Y. Zhang, Z. Jiang, Q. Li, J. Wang, S. Chen and Y. Yang, *J. Solid State Chem.*, 2016, **237**, 274.
24. K. K. Yee, Y. L. Wong and Z. Xu, *Dalton Trans.*,2016, **45**, 5334.
25. Q. K. Liu, J. P. Ma and Y.B. Dong,*Chem. Commun.*, 2011,**47**, 7185.
26. H.M. Zhang, H. Wu, Y.Y. Liu, J. Yang, D. W. Kang and J.F. Ma,CrystEngComm., 2015, **17**, 1583.
27. F.Ke, L.G.Qiua,Y. P. Yuan, F. M.Peng, X. Jiang,. A. J. Xie, Y. H. Shen and J. F. Zhu, *J. Hazard. Mater.*, 2011, **196**, 36
28. F. S. Gentile, M.Pannico, M.Caus`a, G.Mensitieri,G. Di Palma,G.Scherillo and P.Musto, *J. Mater. Chem. A.*, 2020, **8**, 10796.
29. F. Ke, J. Jiang, Y. Li, J. Liang, X. Wana and S. Ko, *Appl. Surf. Sci.*, 2017, **413**, 266.
30. A. K. Kar and R.Srivastava,*New J. Chem.*, 2018, **42**, 9557.
31. Q. Zhao, L. Zhu, G. Lin, G. Chen, B. Liu, L. Zhang, T. Duan and J. Lei, *ACS Appl. Mater. Interfaces.*,2019, **11**, 42635.
32. V. Fierro, V. Torné-Fernández, D. Montané, A. Celzard, *Micropor. Mesopor.Mater.*,2008, **111**, 276.
33. D. K. Kaushik, M. Selvaraj, S. Ramu and A. Subrahmanyam, *Sol. Energy Mater.Sol. Cells.*, 2017, **165**, 52.
34. I. Jerman, V. Jovanovski , A. ŠurcaVuk, S.B. Hočevar, M. Gaberšček, A. Jesih, B. Orel, *Electrochim.Acta.*,2008, **53**, 2281.

Dr. Siddhartha Kolay *has done his M. Sc. in Inorganic Chemistry from the University of Calcutta and joined the Chemistry Division, BARC, in 2007 after graduating from the 50th batch of the training school. He obtained his Ph.D. from Homi Bhabha National Institute, Mumbai, in 2016. His research work is primarily focused on the synthesis of metal-organic frameworks (MOFs) and covalent organic frameworks (COFs) for various applications. His current research interest is the development of radiation-stable MOFs and COFs for nuclear off-gas treatment and heavy metal extraction from nuclear waste.*

Metal–Organic Frameworks for Separation, Capture and Sensing/Detection of Noble Radioactive Gases

Sandeep Kumar Sharma* and Jaideep Mor
Radiochemistry Division, Bhabha Atomic Research Centre, Mumbai 400 085
*E-mail: *skumars@barc.gov.in*

Abstract

Metal Organic Frameworks (MOFs) are crystalline and highly porous materials. MOFs have shown potential applications in gas storage and gas separation due to their high porosity and well regulated pore network. High chemical and thermal stability have enhanced their applications in various fields. MOFs are also shown to have high selectivity and uptake capacity for noble gases which is primarily achieved through fine tuning of pore network of MOFs. High radiation stability of MOFs along with high separation efficiency of noble gases have increased the potential of MOFs in storage and separation of noble radioactive gases which are otherwise released in atmosphere. MOFs showing scintillating properties along with high uptake capacity of noble gases are suitable for detecting and sensing the radioactive noble gases. Herein, we present a review of recent studies focused on MOFs applications in separation, capture and sensing/detection of noble radioactive gases.

1. Metal–Organic Frameworks

Metal–Organic Frameworks (MOFs) represent the tremendous beauty of chemical structures following the concepts of two different disciplines of chemistry i.e. inorganic and organic chemistry. MOFs are highly porous and crystalline materials following the isoreticular chemistry concept of synthesis.[1] Yaghi et al. have reported the first synthesis of crystalline and porous MOFs.[2] MOFs are made of metal nodes linked with organic linkers, and both the constituents of MOFs provide possibilities of large variations. Till date, around 90,000 MOF structures have been synthesised. The crystal structure of MOFs are derived through coordinations between metal ions and organic linkers which exhibit the interconnected pore network leading to higher porosity and large surface area (Figure 1). Till date, a maximum porosity of ~ 90% of total volume and the surface area up to 6000 m^2/g has been reported.[3] In addition, MOFs offers structural flexibility, tunable porosity, variable organic functionality, and very high physical/thermal stability. These exceptional properties of MOFs have led to their applications in different fields viz. energy, sensing and gas storage. Due to the large porosity and well-defined interconnected pore-network of MOFs, they have found tremendous applications in the storage and separation of gases.[4]

As mentioned before, MOFs consist of organic linkers called primary building units (PBU) coordinated with metal ions or clusters called as secondary building units (SBU). Depending on constituent units as well as the resultant structure, MOFs are classified into different groups. For example, isoreticular MOFs consist of $[Zn_4O]^{6+}$ connected to aromatic carboxylate;[5] Zeolitic Imidazolate Frameworks (ZIFs) consist of different metal ions (Zn, Co, Fe, Mn, Cd, etc.) connected to derivatives of imidazolate linkers;[6] Porous Coordination Networks (PCNs) are stereo-octahedron materials having a hole−cage−hole topology with a 3D structure;[7] Materials Institute Lavoisier (MIL) MOFs consists of different elements (Al, Cr) linked with organic linkers having two carboxylic functional groups;[8] Porous Coordination Polymers (PCPs) consists of transition metals linked with carboxylic acid, pyridine, and its derivative;[9] University of Oslo (UiO) MOFs consists of $Zr_6(\mu_3\text{-}O)_4(\mu_3\text{-}OH)$ connected to dicarboxylic acid[10]. In addition, other groups of MOFs have been classified as Northwestern University (NU),[11] Pohang University of Science and Technology (POST-n),[12] Dresden University of Technology (DUT-n family),[13] University of Nottingham (NOTT-n),[14] Hong Kong University of Science and Technology (HKUST-n),[15] and Christian-Albrechts-University (CAU-n family)[16]. Synthesis of MOFs is carried out using different methods viz. room temperature solvent assisted method,[17] electrochemical method,[18] microwave-assisted method,[19] solvothermal method,[20] mechanochemical method,[21] and sonochemical method[22]. The choice of synthesis method of MOF depends on various factors such as the constituent of MOFs (PBU and SBU), topology and crystal size of the product, amount of the product, use of environment-friendly solvents and applications of the product etc. Among the reported method, solvothermal synthesis is preferred to synthesize large-size single crystals of MOFs,

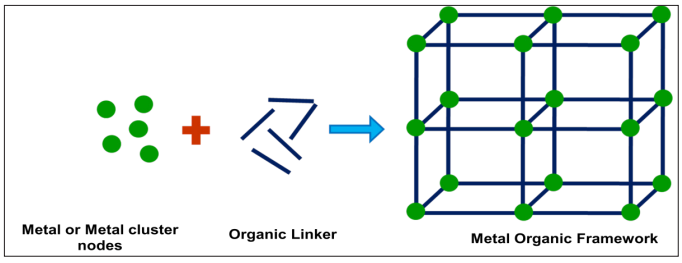

Figure 1. *Schematic showing formation of porous network of metal organic frameworks by coordination of metal or metal cluster nodes and organic linkers.*

whereas mechanochemical and sonochemical methods are considered as high throughput synthesis method. In spite of different synthesis methods, a strong emphasis is always given to the environment-friendly room temperature synthesis method of MOFs.

2. Gas Adsorption and Separation Using Porous Materials

Gas separation is a crucial process for producing the purified gases having applications in different industries, and hence research towards the development of an economical gas separation process is continuously pursued for the separation of different gas mixtures. In general different gas separation techniques such as cryogenic distillation, membrane-based, and adsorption-based technologies are being employed in different industries.[23–25] Cryogenic distillation is an energy-intensive process, hence efforts are continuously being made to develop technologies for gas separation using membrane-based or adsorption-based technologies for the separation of all types of gases. With the development of synthetic zeolites in the 1940s, adsorption-based separation processes have become prominent in the gas separation industries.[26–28] The adsorption-based separation using various adsorbents have become highly useful for H_2 and CH_4 purifications, CO_2 capture, CO removal for fuel cell technology etc. In addition porous materials-based technologies have been developed for the desulfurization of transportation fuels and other processes required for clean environment.

In adsorptive separation processes using porous materials, gas separation efficiently is based on the difference in the adsorption efficiency of the adsorbent towards different gases present in the mixture. In this process, characteristics of the adsorbent in both adsorption equilibrium and kinetics play a deterministic role towards the overall efficiency of the separation process.[29,30] For the real-life application of any porous material for the separation of gases, it should possess high mechanical properties, good adsorption capacity, selectivity, adsorption kinetics and regenerability. In order to achieve all these characteristics, the adsorbent should be highly porous having an interconnected pore network and high surface area that allow adsorbate molecules to approach the interior surface. Porous materials such as zeolites, silica gel, clays, inorganic and polymeric resins, porous organic materials, activated carbons, etc. have been explored for gas separation and some of them are being used in the industries.[26,31–35] As mentioned before the adsorption capacity and selectivity of an adsorbent are two main characteristics that are directly related to the efficiency of the adsorptive gas separation. Both of these characteristics directly or indirectly depend on the type of pores and pore network of the adsorbent as well as the equilibrium pressure and temperature.

The gas separation using porous materials occurs through different mechanisms (Fig. 2). The molecular-sieving mechanism of separation is based on the size/shape exclusion of certain components of the mixture due to the limited aperture size present in the pore network of the porous materials. The kinetic separation mechanism is based on the different diffusing rates of different components of the gas mixture within the pore network of the porous material. The quantum sieving effect is also based on the different diffusing rates of light molecules in the micropores because of the quantum effect. In addition, the equilibrium separation mechanism is based on the preferential adsorption of certain components of the gas mixture leading to the separation of the gases using the porous materials. Various industrially relevant gas separations are carried out following these mechanisms: drying of gases using 3A zeolites and separation of normal paraffins from iso-paraffins using 5A zeolites are the examples of molecular-sieving which is based on the size/shape exclusion mechanism.[27] The separation and production of N_2 directly from the air, CH_4 from CO_2 using a carbon molecular sieve, and removal of N_2 from CH_4 with 4A zeolites for upgradation of the natural gas are the examples of kinetic separation which is based on the diffusing rates of different components of gas mixture within the pore network of porous materials.[24] In the case of separation of light molecules such as H_2, D_2 , T_2 and He through porous materials having micropores comparable to the de Broglie wavelength of these molecules quantum sieve effect becomes crucial and leads to separation of isotopes of these gases. In the case of thermodynamics equilibrium separation, gas-adsorbent surface interaction is highly crucial and determines the separation efficiency. The gas-adsorbent interaction depends on the surface characteristics of the adsorbent as well as the properties like polarizability, magnetic susceptibility, permanent dipole moment, and quadrupole moment of the adsorbate

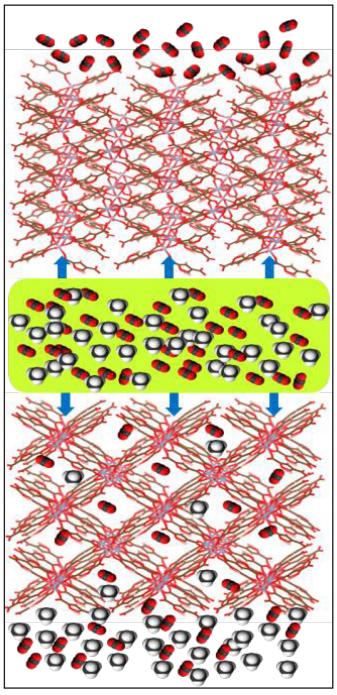

Figure 2. *Gas separation through molecular sieving (Upper Panel) and preferential adsorption mechanism (Lower panel).*

molecules. Li et al.[36] have reviewed the gas separation process using different porous materials with a special emphasis on MOFs.

3. Metal–Organic Framework for Gas Adsorption and Separations

As mentioned earlier, a huge number of scenarios are possible for the design of MOFs based on different combinations of PBU and SBUs. It leads to significant tunability in structure and properties of MOFs which can be systematically realized using the power of organic synthesis. [37–46] As a result, MOFs with very high and well-defined porosity having the specific surface characteristics can be synthesized using very mild conditions. Due to the high porosity and favourable characteristics such as large surface areas, adjustable pore sizes, and controllable surface properties, most of the MOFs are considered as ideal adsorbents for gas storage and separation. In addition, some of the MOFs are highly flexible under stimuli such as temperature, pressure, and the presence of the guest molecules. The flexible frameworks are capable of pressure and temperature-dependent molecular sieving which is not possible for the conventional porous adsorbents. Gas adsorptive separation is a complicated process and depends on the different characteristics of the adsorbents. In the case of MOFs, molecular sieving-based selective adsorption of gases has been confirmed in different MOFs. The molecular sieving effect in the case of MOFs has been attributed to limited aperture size which excludes the larger size gases from adsorption in the pore network. MOFs such as $Mg_3(ndc)_3$,[47] PCN-13,[48] $Sm_4Co_3(pyta)_6(H_2O)_x$,[49] $Cu(F\text{-}pymo)_2$,[50] and $Zn_2(cnc)_2$-(dpt)[51] have shown highly selective adsorption of H_2 over N_2 due to size exclusion. Similarly, $Mg_3(ndc)_3$,[47] Zn(dtp),[52] and PCN-13[48] have shown preferential adsorption of similar molecular size gases (O_2 over N_2) at low-temperature due to size exclusion effects.

As mentioned before, in addition to pore size exclusion, adsorbate-surface interaction also plays a deterministic role in gas-adsorptive separation using porous materials. $Cu_2(pzdc)_2(pyz)$[53] shows preferential adsorption of C_2H_2 over CO_2 due to strong H-bonding between C_2H_2 and O atoms from the surface. Cu(hfipbb)$(H_2hfipbb)_{0.5}$,[54] Zn(tbip),[55] and Zn(bdc)$(ted)_{0.5}$.[56] show preferential adsorption of organics viz. MeOH, EtOH, and dimethylether over water as the channels of these MOFs are highly hydrophobic. $Zn_2(ndc)_2(dpni)$[57] and Mn(ndc) [58] are shown to preferentially adsorb CO_2 over CH_4 due to strong binding of CO_2 having high quadrupole moment at open metal sites in the frameworks (Figure 3). Even though flexible MOFs undergo pore-structure modifications due to framework-gas interaction and gas pressure, they also show significant separation selectivity for different gas mixtures attributed to different factors. For example, Cd(pzdc)(bpee)[59] shows preferential adsorption of water and methanol compared to ethanol, tetrahydrofuran and dimethyl ketone. Selective adsorption of benzene over cyclohexane has been observed in Cu(etz).[60] Similarly, significant selectivity has been observed in propene/propane separation using ZIF-8 and its different derivatives. [61-66] All these preferential adsorption-based separations in these flexible MOFs are attributed to molecular sieving through the modified pore structure. Flexible MIL-53 shows different adsorption characteristics for CH_4 and CO_2 due to different host-guest interactions, and can be used for their separation using hydrated and dehydrated forms of MIL-53.[67] In the case of flexible MOFs, gate-opening under external stimuli has also led to selective separation of gas mixtures having kinetic diameter larger than the inherent pore size. ZIF-20[68] having a pore aperture size of 2.8 Å has shown very high adsorption of CO_2 as compared to CH_4 due to the gate-opening effect. $Cu(dhbc)_2(4,4'\text{-}bpy)$[69] shows that the pressure required for gate-opening under O_2, N_2, and Ar is distinctly different which confirms that gases in this type of MOFs can be selectively adsorbed at different pressures (Figure 4). Similar observations have been observed in different ZIFs viz. ZIF-8, ZIF-7, ZIF-9 and their mixed metal and mixed linker derivatives.[70–76]

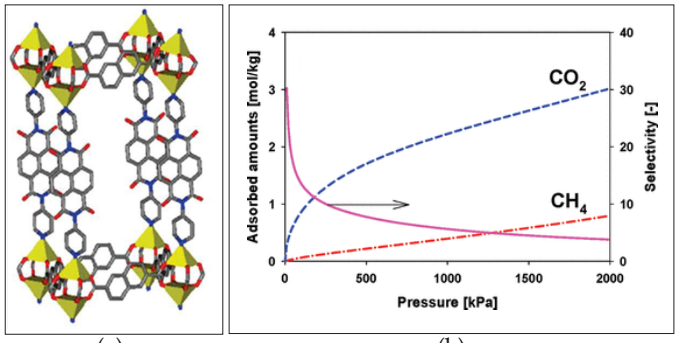

(a) (b)

Figure 3. *(a) Single crystal structure of $Zn_2(ndc)_2(dpni)$; (b) CO_2 and CH_4 uptake capacity and selectivity of $Zn_2(ndc)_2(dpni)$; Reprint with permission from Ref. [57].*

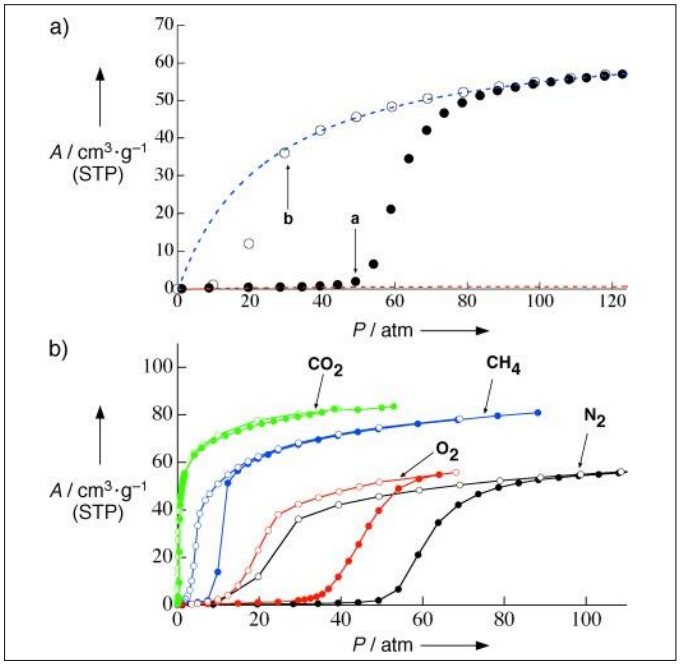

Figure 4. *(a) Nitrogen adsorption (filled circles) and desorption isotherms (open circles) for [Cu(dhbc)2(4,4'-bpy)] at 298 K. Blue and red dashed lines were determined by fitting the linear parts of the Langmuir plots in the higher (from 83 to 122 atm) and lower (from 8 to 34 atm) pressure ranges, respectively; (b) Adsorption (filled circles) and desorption (open circles) isotherms of N_2, CH_4, CO_2 and O_2 at 298 K. (Reprint permission from ref. [69]).*

4. Adsorption and Separation of Noble Gases

The volatile ideal gases specifically Xe and Kr have applications in Lasers and medical devices etc.[77] Their relative abundance in the atmosphere is very low, 0.09 and 1.1 ppm for Xe and Kr, respectively. Currently, these gases are produced from air and separated from each other using cryogenic distillation process which is based on the difference in their boiling points (Figure 5.). [78] The Cryogenic distillation process is highly energy intensive and hence very expensive. In order to reduce the cost of their production and separation, alternative technologies are under development for the separation and preferential adsorption of Xe and Kr. These alternatives are divided into two types (i) selective adsorption by dissolution in an appropriate solvent and (ii) physisorption on porous materials [77–80] The first process is similar to cryogenic distillation but the separation factor depends on the solubility of gases in the solvent which also depends on the temperature and pressure. Some studies using dichlorodifluoromethane (refrigerant-12, R-12) as a process solvent[81] has shown a very high separation factor for ^{85}Kr. Additionally, CO_2 has been proposed as a solvent for the process as it has many advantages as compared to dichlorodifluoromethane. The issues with this process are solvent leakage, volatilization and radiolysis which have to be circumvented before its implementation at a large scale. Another promising alternative for noble gas separation is based on their physisorption on microporous materials having high porosity and large surface areas. These materials offer options for tuning the gas-adsorbent surface interaction sometimes leading to enhancement in the selectivity of gas adsorption. Among porous materials, zeolites have been used to investigate the adsorption and separation of noble gases [79,82]. Zeolites like NaA and NaX show poor selectivity (separation factor 4–6) with low capacities of 20–30%.[82] Commercially available activated charcoals have also been studied for this purpose.[83] However, their applications are not recommended as they pose a fire hazard risk due to the presence of NO_x in the gas stream. As a result of poor selectivity and low capacities and other above-mentioned issues, the above-discussed porous materials are not being used for the capture of noble gases though they are being used for many other types of gas separations based on the adsorption characteristics.[84]

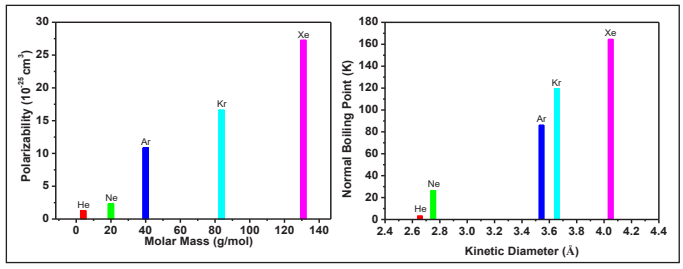

Figure 5. *Thermodynamic properties (Polarizability, Boiling points and kinetic diameter) of noble gases.*

5. Radioactive Noble Gases

Volatile radionuclides are produced during the fission of uranium and plutonium in a nuclear reactor which are released in the off-gas stream of the reprocessing plant during the reprocessing of the nuclear fuel, and finally,

these volatile products are released into the environment with utmost care. These radionuclides are ^{14}C, ^{129}I, ^{3}H and noble gases. The noble gases isotopes produced in the nuclear industries are ^{41}Ar (activation product), ^{85}Kr, ^{87}Kr, ^{88}Kr, ^{133}Xe, ^{135}Xe and ^{138}Xe. The volatile radionuclides in the off-stream of a reprocessing plant operated on aqueous reprocessing of the spent fuel contain mixture of noble gases along with tritiated water, different forms of iodine ($H^{129}I$, $^{129}I_2$, and organic iodides). In general, iodine and tritium are captured from the off-stream whereas CO_2 and Kr are released in the environment.[84] In order to reduce the radioactive hazard to the environment, separation and capture of noble gases (Kr and Xe) is highly important. The capture of these gases becomes more important for molten salt breeder reactors where the gaseous fission product reaches to the headspace of the reactor because of its particular type of design. These gases are swept away by the cover gas, and have to be captured to clean the cover gas. For the capture and separation of these noble gases, the most promising process would be capable of separating these gases from the air as well as from each other at room temperature and pressure.

In the case of reprocessing plants, off-stream primarily contains only non-radioactive Xe because of a short half-life of ^{127}Xe (36.3 days). As a result of short half-life, ^{127}Xe becomes nonradioactive during the cooling period of the spent fuel which is approximately 5 years and longer. However, ^{85}Kr having long a half-life (10.8 years) remains present in its radioactive form in the off-stream. Xe production is 10 times higher than Kr during the fission process. Hence, ^{85}Kr should be captured and stored to reduce the release of radioactivity in the environment, and Xe separation is required to reduce the waste of noble gases which have potential applications in various industries.

Another radioactive noble gas of concern is radon (Rn) which is a component of air and it is the major fraction (~ 40%) of the natural radiation to the public[85] Radioisotopes of Rn (^{219}Rn, ^{220}Rn, and, dominantly, ^{222}Rn) are produced in the natural decay series of ^{235}U, ^{232}Th, and ^{238}U.[86] Rn is present in the ultralow concentration in air but it is encouraged to control the radiation exposure to Rn radiation as low as possible especially in radioactive laboratories where Rn concentration may be high. In addition, Rn concentration control in air is also required for rare event physics experiments wherein decay of Rn can create a spurious pulse.[87] The techniques currently used for Rn activity control are either physical blocking or ventilation-based but these techniques are expensive and not very efficient. Hence, new economical methods based on adsorption by porous materials are being developed for capture of Rn from air.

6. Metal Organic Frameworks for Radioactive Noble Gases

6.1. Xe capture and Xe/Kr separation

As mentioned before, some of the porous materials such as zeolites and activated carbons have been explored for the separation of noble gases. The storage capacity of these materials was observed to be very limited, and could not be enhanced as tuning of their pore architecture is not possible. On the other hand, MOFs consist of metal nodes connected with organic linkers providing ample opportunities for fine-tuning the pore architecture of the frameworks. In the case of MOFs, pore architecture is determined by coordination modes, geometry, directionality, and functionality of linkers as well as synthetic conditions. As a result, the pore architecture of MOFs can be easily tuned for specific purposes. Till date, many interesting studies have been performed for noble gas adsorption and separation using MOFs which are discussed below.

One of the first studies related to the application of MOFs for noble gas adsorption was performed by Muller et al.[88] using IRMOF-1[1]. Their study confirmed that a stainless steel container filled with IRMOF-1 can contain more moles of noble gas as compared to an empty cylinder. The study also showed a significant difference among different noble gases based on their polarizability. Muller et al. have also explored to application of another interesting MOF i.e. HKUST-1[1] for separation selectivity of Kr/Xe. HKUST-1 is copper-based MOF having a porous network and accessible Cu metal sites.[89] Using HKUST-1 as an adsorbent, a significant improvement in the separation selectivity of Xe/Kr as compared to activated Carbons has been obtained. However, commercially available HKUST-1 showed lower Xe capacity (3.18 mol/kg) as compared to activated carbons (3.72 mol/kg).[90] Interestingly, HKUST-1 shows good adsorption capacity of noble gas from air which indicates its suitability for applications in off-stream gases of nuclear reprocessing plants. The adsorption sites of noble gases in HKUST-1 were confirmed to be the small pockets and the surrounding windows leading to the cavity through investigations using NMR, X-ray and neutron scattering analysis.[89,91] The pore structure of FMOFCu consists of tubular cavities (~ 0.51 × 0.51 nm) connected to smaller size windows of dimensions 0.35 × 0.35 nm. This particular MOF could be used to selectively adsorb Kr (kinetic diameter 0.36 nm) over Xe (kinetic diameter 0.39 nm) using the molecular sieving effect. The selective adsorption of Kr using FMOFCu was observed at 0 °C and lower temperature as at higher temperatures, expansion of the window permitted the diffusion of Xe also within

the pore network of the MOF. [92,93] DOBC-based (DOBDC = 2,5-dihydroxyterephthalate) MOFs with different metal nodes (M = Mg, Mn, Fe, Co, Ni, Zn) are highly porous having open metal sites .[94] As a result, these MOFs are excellent beds for adsorption of different gases. Ni-DOBDC has shown 55 and 3 wt.% adsorption capacity for Xe and Kr, respectively at 100 kPa and 298 K. The adsorption capacity for Xe of Ni-DOBDC is comparable to activated carbons. The adsorption performance of DOBDC-based MOFs was found to be independent of metal nodes.[95] The adsorption capacity and selectivity (Kr/Xe) could be enhanced by loading Ag nanoparticles in Ni-DOBDC.[96] Ag-loaded MOFs showed Xe uptake capacity of 70 wt.% and Xe/Kr selectivity of ~ 7. The observed enhancement is attributed to the strong dipole-induce dipole interaction between the noble gases and Ag nanoparticles. Combining Ni-DOBDC and FMOFCu in a two-step process, Xe and Kr were efficiently separated.[97] MOFs based on formats linkers $M_3(HCOO)_6$ (M = Mg, Ni, Co, Zn, Mn) with pore sizes of 0.5–0.6 nm of zig-zag channels have also been explored for the adsorption characteristics towards noble gases.[98,99] $Co_3(HCOO)_6$ shows type I and liner adsorption isotherms for Xe and Kr.[98] Separation selectivity of ~ 6 for Xe has been observed for the formate-based MOFs. The separation selectivity has been attributed to the zig-zag channels of these MOFs as Xe atoms fit preferentially at one site of these zig-zag channels. MOF-505 was tested for the breakthrough experiments based on the computational results that showed Xe/Kr separation selectivity using MOF-505 in the pressure range of 0.1 to 1 MPa.[92,100] MOF-505 showed preferential adsorption of Xe as compared to Kr resulting in separation selectivity of 9–10. In this case, preferential adsorption of gases was attributed to the pore confinement effect as well as polarizable open metal sites present in the pore network of this framework.

Xiong et al.[101] have studied the noble gas separation performance of a microporous MOF i.e. MOF-Cu-H which has the suitable pore size matching with the size of Xe. The organic linker for MOF-Cu-H is H_2PYBDC (H_2PYBDC = 5-(pyridin-3yl)-1,3-benzenedicarboxylic acid). In this particular MOF, the pore network consists of one-dimensional (1D) distorted rhombic channels with a size of ~ 6.4 Å. However, due to the presence of stretched pyridine rings from the $PYBDC^{2-}$ anions into the channel, 1D channel is divided into two smaller parts of sizes ~ 3.7 Å In addition, the pore network of the MOF consists of small size cages of sizes ~ 4.4 Å with window openings of 3.5 Å that connects these pores to the 1D channels The size of these pores are precisely matching with the kinetic diameter of Xe (4.1 Å). Investigation of MOF-Cu-H under dilute conditions (< 500 ppm Xe) pertinent to nuclear fuel reprocessing showed good adsorption kinetics, high Xe adsorption capacity (3.19 mmol/g at 1 bar and 298 K) and significantly high Xe/Kr separation selectivity (~ 16). The outstanding performance of this MOF for noble gas separation is attributed to the specially designed pore network as it does not contain any open metal site.

Lee et al.[102] have studied three different MOFs viz. (MIL-100(Fe), MIL-101(Cr), and UiO-66(Zr)) for the noble gas separation. From the Xe and Kr isotherms, it was observed that among all three, UiO-66(Zr) has the highest adsorption capacity (1.18 mmol/g) for Xe at 1 atm and 298 K. In these MOFs, smaller pore size was observed to result in higher adsorption capacity because the adsorption strength increases with the increase in overlap of the potential field from two opposite walls of the pore. The dynamic breakthrough experiment using UiO-66(Zr) pellets showed Xe/Kr selectivity of 3.8. The observed selectivity is comparable to the Xe/Kr gas selectivity of other MOFs. UiO-66(Zr) based column has shown very good regeneration just by purging it for 30 min under a He flow of 30 ml/min without heating the column. In addition, UiO-66(Zr) has shown very high hydrothermal and radiation stability which are important criteria for a porous material to be used for noble gas adsorptions from off-stream gases of a processing plant.

Niu et al.[103] (Figure 6) have reported a self-adjusting MOF (ATC-Cu) for the capture of Xe and Kr at very low partial pressure, a condition similar to nuclear reprocessing plant. ATC-Cu structure consists of a 4 Cu paddle-wheel connected by the ATC linker to construct a 4,4-coordinated network. The pore network of ATC-Cu consists of two types of cavities (I and II), and also contain the open metal sites. The average radius of these cavities is 3.90 and 3.85 Å, respectively. Xe was observed to be adsorbed at the centre of these cavities leading to a reduction in size of these cavities. At 298 K, the Xe and Kr uptake capacity of

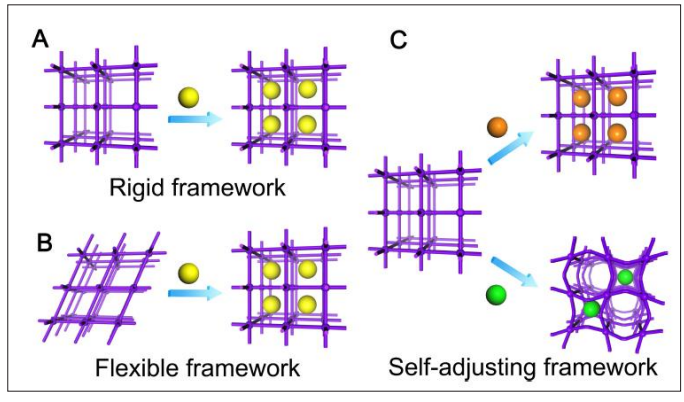

Figure 6. *Schematics showing the structure of rigid (A), Flexible (B) and self-adjusting frameworks (C). Reprint with permission from ref [103].*

this MOF are 5.0 & 2.65 $mmolg^{-1}$, and 2.7 & 0.52 $mmolg^{-1}$ at 1 and 0.1 bar, respectively. The Xe adsorption capacity at 1 bar for this MOF is much higher than Xenon hydrates. The cycle performance of this MOF for the adsorption of noble gases is very excellent. The adsorption capacities for noble gases at low pressure and ambient conditions for this MOF are comparable with the available materials showing the best capacities and hence, it is a promising material for removal of the noble gases from the off-stream of a nuclear processing plant.

Chen et al.[104] have investigated the Xe/Kr separation performance of a microporous MOF i.e. SBMOF-2.2H_2O (Stony Brook MOF-2). This MOF has a rigid three-dimensional crystalline structure consisting of Ca metal nodes connected to a linker 1,2,4,5-tetrakis(4-carboxyphenyl)-benzene. The dehydrated form of SBMOF is highly porous and has ~ 25.6 % of void space in its unit cell. The hydrated state of SBMOF-2 shows a high Xe capacity of ~ 27 % at 298 K along with a high Xe/Kr selectivity of approximately 10 at 298 K. SBMOF-2 shows type I adsorption isotherms for both Xe and Kr but the adsorption capacity for Xe is 3 times higher than Kr. Through diffraction measurements, two sites for adsorption of Xe and Kr have been identified in this MOF. In the same series, Banerjee et al.[105] have investigated the performance of SBMOF-1 which is also known as CaSDB, [SDB = 4,4-sulfonyldibenzoate] for the separation and capture of Xe. In this study, SBMOF-1 was chosen after a rigorous molecular dynamic (MD) simulation screening of existing and newly predicted MOFs. Xe uptake at lower pressure using activated SBMOF-1 was observed to be very close to the predicted value from the MD simulations. The saturation of isotherms for Xe at lower pressure as compared to other gases like Kr confirmed the preferential adsorption of Xe in SBMOF-1 which is a requisite for higher separation selectivity. Xe uptake in SBMOF-1 was observed to be very fast reaching ~ 80 % within the first 10 minutes. Additionally, it retained its adsorption capacity after 10 adsorption/desorption cycles confirming its superior performance under multiple cycles. A single breakthrough experiment performed on SBMOF-1 using a representative gas mixture (400 ppm. Xe, 40 ppm. Kr, 78.1 % N_2, 20.9 % O_2, 0.03 % CO_2 and 0.9 % Ar) showed preferential capture of Xe by SBMOF-1. All other gases pass through column within minutes, whereas Xe is retained in the column for hours. The Xe uptake capacity under dynamic conditions was observed to be 13.2 mmol Xe per kg which is significantly higher than many MOFs and porous materials used for this purpose. SBMOF-1 also showed remarkably high Xe uptake (~11.5 mmol kg^{-1}) even in the presence of water vapor. The remarkable performance of this MOF in the presence of water vapour is attributed to the absence of an open metal site in this framework.

Liu et al.[106] have recently reported an ultra-microporous MOF for the Xe adsorption and separation having a benchmark performance. The ultramicroporous MOF i.e. Cu-MOF-11 was synthesized using H_4ATC (1,3,5,7-adamantane tetracarboxylic acid) and copper nitrate trihydrate [$Cu(NO_3)_2 \cdot 3H_2O$] through a hydrothermal reaction. The 3D network of MOF-11 consists of ATC linker connected with four $Cu_2(COO_4)$ metal clusters, and each metal cluster connected to four linkers. This type of linkage results in a porous network consisting of two types of channels: one square-shaped channel (diameter 4.4 Å) along the z-xis and another rhombic channel (diameter 4.4 × 5.4 Å) along the x and y-axis. In addition to these channels, two aliphatic hydrocarbon cavities also exist in the pore network wherein 8 or 12 hydrogens from the linker point toward the centre of cavities. The distances between these hydrogens in the cavities is ~ 3.5 and 3.7 Å, and hence provide potential adsorption sites for the adsorption of Xe. The total adsorption capacity for Xe of this MOF at 1 bar and 298 is determined to be 4.95 $mmolg^{-1}$, which is among the best capacities reported for different porous materials. This particular MOF shows highly temperature-dependent adsorption isotherms and saturation at very low pressure. These characteristics indicate its very strong affinity for the Xe adsorption. The uptakes for other various gases (Kr, Ar, N_2 and O_2) under the same conditions (298 K and 1 bar) by MOF-11 are observed to be very low, which indicates its preferential adsorption characteristics for Xe. MOF-11 showed the highest storage density (3533 g/L) of Xe at 200 K. The Xe/Kr separation selectivity for a 20/80 binary gas mixture was determined to be ~ 19.1 at 298 K and 1 bar based on ideal adsorbed solution theory (IAST). Thus determined selectivity is among the highest for the studied MOFs till date. Single crystal diffraction studies on Xe-loaded MOF-11 confirmed a very dense packing of Xe atoms within the cavities of the frameworks. The breakthrough experiment at 298 K for a representative Xe/Kr (20/ 80) gas mixture resulted in Xe/Ke separation selectivity of ~ 16.6 which is one of this highest. During the desorption process, high-quality Xe could be produced with a very good recovery rate. The regeneration capacity of MOF-5 during the breakthrough experiments involving multiple cycles was found to be extraordinary. In view of its superior performance for Xe/Kr separation, MOF-11 was tested mimicking the conditions of the off-stream gases of a reprocessing plant. Under the very dilute conditions of noble gases in the feed mixture, the Xe adsorption capacity was observed to be 24.5 mmol kg^{-1} at 298 K which is again highest among all the porous materials used for

this purpose. MOF-11 also showed extremely high stability under harsh conditions similar to the off-stream of nuclear reprocessing plant.

Hurley et al.[107] have studied four Al-based robust MOFs for the adsorption and separation of noble gases. The sizes of the pores present in these frameworks [Al-PMOF, Al-PyrMOF, Al-BMOF and MIL-120] are decided by the dimensions of the tetracarboxylate ligand. Hence the longer ligand results in MOF with larger pore size. Among these four MOFs, MIL-120 has the least surface area (177 m^2/g) whereas Al-PMOF has the highest surface area (1339 m^2/g). All these MOFs show preferential adsorption capacity for Xe as compared to Kr due to the compatibility of Xe with the pore sizes of the frameworks. At 1 bar Xe pressure and 298 K, Al-PMOF exhibited the highest capacity of 5.28 mmol/g among all the four Al-MOFs. The lower capacity exhibited by Al-PyrMOF is attributed to the flexibility of this framework under gas pressure. The Xe selectivity using IAST theory was predicted highest for MIL-120 at low pressure (< 5 mbar) whereas it was higher for Al-BMOF. The breakthrough experiment using a single column was performed on a He gas containing 400 ppm Xe and Kr mimicking the off-gas stream of a nuclear reprocessing plant. No retention of Kr was observed in the column whereas significant retention of Xe was observed. Xe capture by Al-BMOF was observed to be three times higher as compared to MIL-120. Exposure to acidic and basic conditions confirmed higher stability of Al-BMOF as compared to MIL-120.

Idress et al.[108] have investigated the Xe/Kr separation using a Zr-based MOF (NU-403) tailoring its pore aperture and structural defect. NU-403 structure consists of Zr_6-clusters linked with 3D bicyclo[2.2.2]octane-1,4-dicarboxylate. The pore aperture of NU-403 (~ 5 Å) was observed to be smaller than UiO-66 (~ 7 Å). NU-403 was treated with a post-synthetic healing process to prepare a defect-free NU-403-PSDH. Both UiO-66 and NU-403-PSDH showed good adsorption capacity of noble gases at 298 K because the pore sizes of both frameworks are larger than the kinetic diameter of Kr and Xe. However, uptake of Xe at lower pressure was observed to be much higher by NU-403-PSDH as compared to UiO-66 indicating the possibility of better separation selectivity of Xe from Kr at lower pressure using the newly synthesized MOF. The separation selectivity for Xe from a 20:80 Xe:Kr mixture based on IAST using the gas adsorption isotherms was determined to be ~ 6 for UiO-66. The separation selectivity was observed to be reduced to ~ 2 for NU-403 due to the linker defects which increases the pore size. However, defect-healed NU-403-PSDH showed the Xe/Kr separation selectivity of ~ 9 due to the improved pore confinement of Xe in the smaller size pores.

Meek et al.[108,109] have explored the role of polarizability on the adsorption of noble gases in isoreticular MOF (IRMOF-2). To vary the polarizability of IRMOF-2, hydrogen in the linker has been replaced with different halogens (−F, −Cl, −Br, or −I). The framework structure of these halogenated MOFs remains nearly identical to their hydrogenated counterpart i.e. IRMOF-1. The surface area, pore volume and pore size etc. were observed to be nearly the same for all the halogenated MOFs. In this study, it was observed that increasing polarizability leads to an enhancement in the adsorption uptake of the gases.

Gong et al.[110] have investigated the nanoporous carbons derived from ZIF-11, [$Zn(bIM)_2$], for the separation selectivity and adsorption characteristics of Xe. The nanoporous carbons were derived by heating ZIF-11 under high-purity nitrogen gas at 700, 800, 900, 1000 and 1100 °C for 8 hours followed by their washing with HF to remove the Zn metal from the derived carbons. Another series of nanoporous-derived carbons were synthesized following the above-mentioned procedure for composite of ZIF-11 and furfuryl alcohol (FA) composites. It is shown that nanoporous carbon derived from the composite by heating at 1000 °C exhibits the best characteristics for Xe separation and capture from the gas mixture having dilute Xe content mimicking the off-stream of a nuclear reprocessing plant. The nanoporous carbon derived from the composite by 1000 °C heating shows a thermodynamics selectivity of ~ 19.7 at dilute conditions. The nanoporous carbon also showed a very high adsorption capacity of Xe (20.6 $mmolkg^{-1}$) under dilute dynamics conditions (350 ppmv Xe, 35 ppmv Kr, 78% N_2, 21% O_2, 0.03% CO_2 and 0.9% Ar). These characteristics indicate that the nanoporous carbons derived from ZIF-11 in this study are excellent materials for noble gas capture and separations.

Pei et al.[111] (Figure 7) have investigated the robust and radiation-resistance Hoffman-type MOFs for their utilization in the separation of Xe/Kr and capture of Xe from dilute off-gas streams. Two Hoffman-type MOFs Co(pyz)[$Ni(CN)_4$] (termed as ZJU-74a-Ni) and Co(pyz)-[$Pd(CN)_4$] (termed as ZJU-74a-Pd) were prepared and investigated. These MOFs have a porous framework consisting of pore sizes (4.1 and 3.8 Å) comparable to the kinetic diameter of Xe (4.047 Å) and oppositely placed adjacent open metal sites for preferential adsorption of Xe compared to other gases. These MOFs showed unprecedented Xe uptake capacities (89.3 and 98.4 cm^3 at 296 K) at 0.2 bar. The uptake capacities at lower pressure (0.2 bar) are nearly 89.6% and 93.4% of their Xe uptake capacities at higher pressure (1

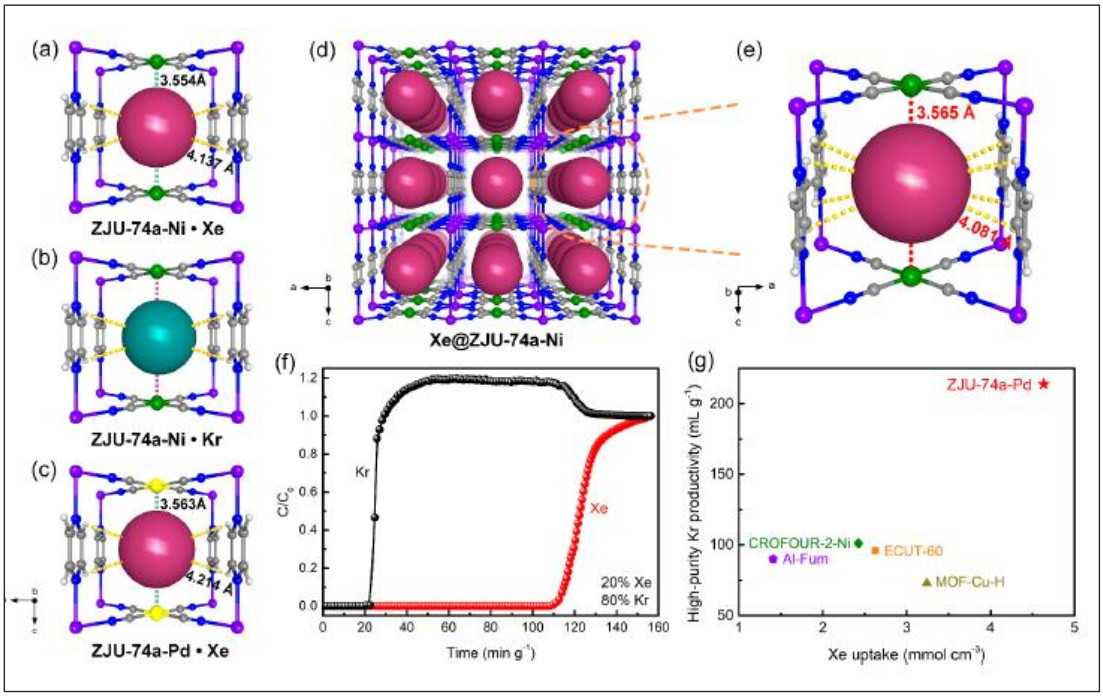

Figure 7. *Theoretical simulation of binding sites of (a) Xe and (b) Kr in ZJU-74a-Ni, and (c) Xe in ZJU-74a-Pd. (d) SCXRD structure of Xe loaded ZJU-74a-Ni. (e) Xe adsorption site in ZJU-74a-Ni illustrated by SCXRD. (f) Breakthrough curves of 20/80 Xe/Kr for ZJU-74a-Pd using gas flow of 2.5 mLmin^{-1} and 1 bar. (g) Xe uptake comparison by different MOFs. Reprint with permission from Ref.* [111]

bar). Such high adsorption capacity at lower pressure confirms their high selectivity for Xe/Kr separation. It was confirmed from SCXRD analysis of the Xe adsorbed ZJU-74a-Ni that one Xe molecule per unit cell is adsorbed which finally corresponds to 4.52 mmol cm^{-3} gas. Thus determined uptake capacity was observed to be consistent with the experimentally determined Xe uptake (4.45 mmol cm^{-3}) at 296 K and 1 bar. The dynamic breakthrough experiment was performed to determine the separation performance of ZJU-74a-Pd for an actual 20/80 Xe/Kr mixture. Kr breakthrough occurs at 24 min g^{-1} whereas Xe breakthrough occurs much later at 110 min g^{-1} confirming its potential for the separation of these gases. These MOFs showed full adsorption capacity regeneration after 3 cycles confirming their reusability. The crystallinity of ZJU-74-Pd remains maintained after exposure to a high dose of 1000 kGy that confirms its high radiation stability compared to other materials proposed for the noble gas separation from the off-stream gases of the nuclear reprocessing plants.

Perry et al.[112] have investigated the noble gas adsorption characteristics of ten different MOFs. In the first series MOF-74-x series (x = Mg, Co, Ni, and Zn), the effect of divalent metal (x) identity within a constant topology was explored. The second series consists of nbo-MOFs, and in this case the effects of pore size maintaining constant open metal sites on gas adsorption characteristics have been explored. Gas uptake by nbo-MOFs was observed to increase with decreasing pore size. This trend in gas uptake is attributed to the gas polarizability as highly polarised gas atoms are strongly confined in smaller pore sizes. A systematic investigation focused on the pore architecture vs gas uptake confirms that large cages connected with narrow pores efficiently adsorb the noble gases as such pore network provides a tortuous, zig-zag diffusion pathways that likely increase the strength of the MOF-gas interaction. The investigation focused on the role of open metal sites confirms that the accessibility of open metal sites enhances the gas-framework interaction largely due to (point charge)-(induced-dipole) interactions. As the charge on divalent metals is same in all the investigated MOFs, insignificant differences in noble gas uptake were observed among the studied MOFs.

Wu et al.[113] have studied the Xe/Kr separation using a Ca based MOF consist of unsaturated Ca centre. The studied MOF viz. Ca-SINAP-1 (SINAP = Shanghai Institute of Applied Physics, Chinese Academy of Sciences) consist of the structure formed by the linkage of Ca metal nodes with the linker 1,1,2,2-tetra(4-carboxylphenyl)ethylene. The porous network of the framework consists of 1D rhombohedral channels with aperture size of ~ 4.8 Å × 13.6 Å. The porous network of the MOFs contains open holed accessible to Xe and Kr atoms. The MOF retains its crystal structure in the dehydrated state, which has been used to study the adsorption characteristics of noble gases as an adsorbent. Ca-SINAP-1 was observed be chemically stable in harsh environment as well as under hydrothermal

conditions. These studies established the fact that this MOF is suitable for application of noble gases from the harsh environment of off-stream gases from nuclear reprocessing plants. The dehydrated form of Ca-SINAP-1 showed Xe adsorption capacities of 54.3 mL/g at 313 K and 100 kPa, which corresponds to the gas occupancy of 1.55 Xe atoms per cell unit. There was no change in the Xe uptake capacity after β irradiation of the MOF confirming its radiation stability which is a prerequisite for the application of a MOF in a nuclear reprocessing plant.

Yan et al.[114] have synthesized two Al-based MOFs i.e. Al-Fum (Al-fumarate, Basolite A520) and Al-Fum-Me (Al-methyl-fumarate). Methyl functionalization of the linker was used to tailor the pore size of the MOF for enhancing the affinity of this MOF towards noble gas adsorption. The Xe uptakes by Al-Fum and Al-Fum-Me were determined to be 3.47 and 3.01 mmol g^{-1}, respectively (298 K and 1 bar). Xe uptakes by these MOFs were observed to be 3.4 and 2.5 times higher than the Kr uptakes under the same conditions. However, the Xe uptakes by these MOFs were comparable with the highest reported Xe uptakes by other MOFs. At lower pressure (0.2 bar) and 298 K, Al-Fum-Me was observed to adsorb higher amount of Xe (1.77 mmol g^{-1}) than that of Al-Fum (1.51 mmol g^{-1}). The steep adsorption of Xe at lower pressure indicates its higher affinity of Xe adsorption resulting in higher separation selectivity for Xe/Kr mixture. The isosteric heats of adsorption for Xe adsorption at Al-Fum-Me was determined to be higher than Al-Fum confirming the strong binding of Xe with Al-Fum-Me. The Xe/Kr separation selectivity factors of 10.0 and 8.1 for Al-Fum-Me and Al-Fum were determined using IAST theory. Higher separation factor for Al-Fum-Me clearly indicates the narrowing of pore size due to steric hindrance caused by the methyl functionalization of the linker has a direct role in the separation selectivity of the gas mixture. Single-column breakthrough experiments performed at 298 K using Al-Fum-Me for 20:80 Xr-Kr binary mixtures showed much faster elution of Kr ~ 4 min g^{-1} as compared to Xe ~ 28 min g^{-1}. These results along with good radiation stability established that Al-Fum-Me can be a suitable candidate for the noble gas capture and separation from the off-stream gases from the nuclear reprocessing plants. Under the dilute conditions (35 ppm Kr, 350 ppm Xe, 21% O_2, 78% N_2, 0.03% CO_2 and 0.9% Ar), Xe capture capacity of Al-Fum-Me was determined to be 5.67 mmol kg^{-1} which is comparable to other MOFs suitable for the application of noble gas capture from off-stream of nuclear reprocessing plants (Figure 8).

6.2. Radon capture

In addition to applications in capture and separation of Xe and Kr, MOFs have also been explored for the capture of radioactive Rn (^{219}Rn, ^{220}Rn, and, dominantly, ^{222}Rn) which is generated through the natural decay series of ^{235}U, ^{232}Th, and ^{238}U. Capture of radioactive Rn from the atmosphere is a big challenge because it has very low partial pressure (<1.8 × 10^{-14} bar, <10^6 Bq/m^3) in air, and interacts only through the weak van der Waals (vdW) interactions with the adsorbent.[115] In such a case, adsorbents having only favorable adsorption thermodynamics or feasible diffusion kinetics do not perform well for Rn capture. For efficient capture, porous materials having both favorable adsorption thermodynamics and feasible diffusion kinetics are required for the efficient Rn capture. Zeng et al.[116] have screened 23 MOFs using computational methods for Rn capture. In this study, four MOFs viz. ZIF-12, HKUST-1, IRMOF-62 and ZIF-11 were proposed as excellent candidates for the capture of Rn. These materials showed a decrease in the separation selectivity of Rn from the gas mixtures with the increase in Rn content. It established that these MOFs are good candidates for capturing Rn from atmosphere having its low concentration. Among these four MOFs, ZIF-12 was observed to have selectivity of ~2800 and 1750 from Rn/N_2 and Rn/O_2 mixtures, respectively having Rn molar concentration of 0.0001.Wang et al.[115] have screened out Imidazole loaded ZIF-7 (ZIF-7-Im) as a promising variant using computer simulation for Rn capture. ZIF-7-Im was shown to have 28 times higher Xe adsorption capacity compared to pure ZIF-7, confirming the role of modified pore network on Xe capture which can be used to mimic the Rn capture in the absence of pure Rn for the adsorption characteristics. The breakthrough experiment performed at 298 K using ^{222}Rn showed an

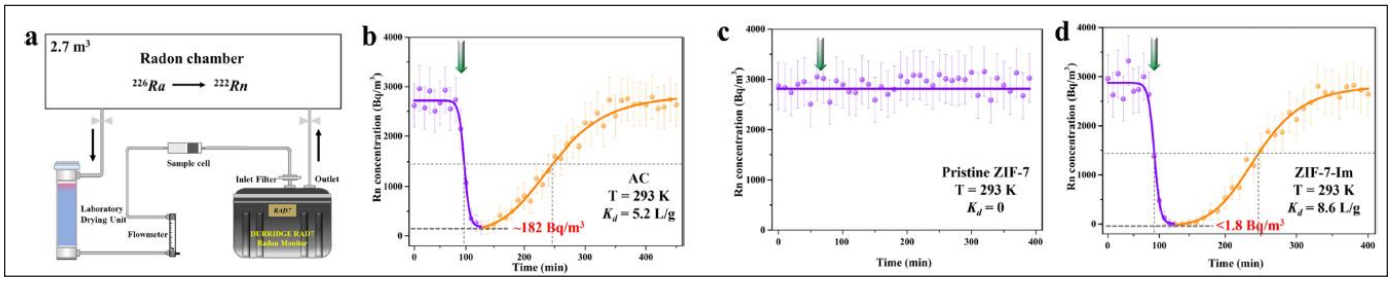

Figure 8. *Schematic showing the capture and separation of Xe and Kr using porous materials from the off-stream of nuclear reprocessing plants.*

efficient capture of Rn as the concentration in the outlet reach below detection level by injecting 3000 Bq/m^3 in the inlet (Figure 9). Park et al.[117] have also followed the same methodology for designing a MOF for the efficient Rn capture. Using computational screening of 4951 MOFs, Al-ndc (ndc = 1,4-naphthalenedicarboxylic acid) was selected for the Rn capture from air. The hydrothermal and chemical stability of Al-ndc were observed to excellent. Using a single breakthrough experiment, Rn removal rate (~ 52.1%) exhibited by Al-ndc was found much higher than the activated carbon (~ 25.3%) confirming its suitability for the Rn capture from the atmosphere.

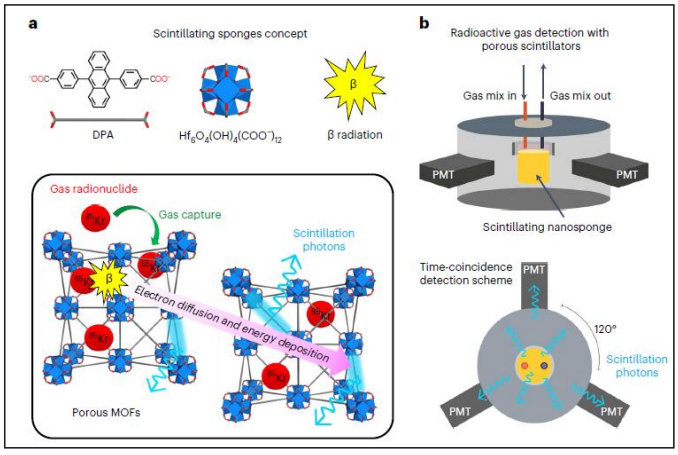

Figure 9. *Profiles of Rn breakthrough experiments* **(a)** *set-up for measurement of Rn breakthrough experiment;* **(b)** *breakthrough experiment using activated carbon at 293 K;* **(c)** *breakthrough experiment using pristine ZIF-7 at 293 K; and* **(d)** *breakthrough experiment using Im-ZIF-7 at 293 K. Reprint with permission from Ref. [115]*

6.3. Sensing and Detection of Radioactive Noble Gases

As discussed before, MOFs have high affinity for capture of radioactive noble gases even from the dilute streams due to their strong binding with noble gases that are attributed to their specially designed pore architecture as well as open metal sites. In addition, MOFs potential for sensing and detection of radioactive noble gases have also been explored designing special types of MOFs. Ionizing radiation (e.g., X-ray, ***γ***-ray, ***β***-ray, ***α***-particle, and neutron) responsive MOFs have been synthesized exploiting the synergy between high atomic number metal nodes and their linkage with the organic linkers.[118] These radiation responsive MOFs efficiently convert the ionizing radiation energy to visible light or electrical charges which is measured using advanced electronics for sensing and detection of these radiations. Whenever the incoming energy of radiation is higher than ionization potential of constituent elements of MOFs, metal nodes or organic linkers undergo ionization leading to creation of electron-ion pair. Thus created high energy electrons produce secondary electrons and electron-hole pair during the thermalization process. The nano-porosity of MOFs allows to accommodate the guest molecules which facilitate the charge transfer and ion conduction through MOFs. MOFs are in general electrical insulator due to their particular type of coordination between metal and linkers. The charge transport in MOFs happens through three different mechanisms; (i) through-bond charge transport, (ii) between linkers charge transport, and (iii) guest-assisted charge transport.[119] For example, Ni-DABT ((DABDT = 2,5-diamino-1,4-benzene dithiol dihydrochloride) exhibit electrical conductivity of 4.0×10^{-7} S cm^{-1} at 300 K which is attributed to the π–d coupling interactions of Ni^{2+} cations and the redox-active amino/sulphydryl groups of $DABDT^{2-}$ linkers. As a result of these characteristics, Ni-DABT shows efficient conversion of X-rays to moving charge carriers.[120] The second mechanism is related to continuous charge transport through non-covalent interactions between the organic linkers which will be stronger in the case of regular packing of linkers. SCU-12 MOF $[(CH_3)_2NH_2]Tb_2(C_6Cl_2O_4)_3(DMF)_2(H_2O)_2(HCOO)$ [17] is one of the examples showing electron transport through linkers only as the negligible overlap between the metal ion and the linker exists in this MOF. Third type of electron transport mechanism is observed in MOFs wherein the pores are occupied by conductive guest molecules. N,N′-diethyl-4,4′-bipyridinium cation (EV^{2+}) viologen unit into the pore of pristine $[(Me_2NH_2)_3(SO_4)]_2[Zn_2(ox)_3]$ MOF is a unique example showing the guest assisted charge transport in MOFs.[121] As a result of electron accepting nature of viologen, strong donor accepter interaction exists between host and guest molecule which finally facilitate the charge transport through the pore network of this MOF. In this case, conductivity of 1.79×10^{-9} S cm^{-1}, is determined under X-ray irradiation which is one order higher than the conductivity measured in the absence of X-rays.

As mentioned before, another mechanism to detect the radiations using MOFs is to convert the radiation energy into light photons. The radiation to light photon conversion can originate from metal ions or linkers. In the case of metal ions with no unpaired electrons, emissions primarily emanate from linkers only. These emissions are similar to what is observed in the solution state of linkers and occur through π–π^* or n–π^* transitions.[122] Metal based emissions are generally observed from MOFs consist of luminescent lanthanide ions or actinide ions which show f-f and d-f transitions.[123] In addition, due to higher Z of these metals as compared to transition metals, they have larger energy absorption coefficient. As such, weak crystal field surrounding the dopants lanthanide ions

pose a challenge in case of MOFs leading to low quantum yield. However, properly designed MOFs wherein energy transfer pathways are facilitated by the linkers show strong radioluminescence. For example, Tb(oxalate)(coo)(1,10- phenanthroline)·H_2O MOF containing 1,10-phenanthroline has been reported as a strong green X-ray scintillator as the linker of the MOF acts as energy transfer agent.[73] It has been shown that exploiting the similar coordination of different lanthanides, MOFs with hybrid lanthanide nodes can produce the emission color gamut.[124,125] In some cases, MOF shows better radiation and hydrothermal stability as compared to a standard CsI:Tl scintillator. Hence, MOFs can be considered as advanced scintillation materials for detection of energetic radiations.

Linker based emission is also possible in MOFs which is utilized for their application as scintillation material for radiation detection. Linkers based benzene derivates are short and, results in the formation of dense MOF which is effective in radiation adsorption. Pb(2-MTA)(DMF) MOFs (denoted as SCU-200, 2-MTA = 2-methylterephthalic acid, DMF = N,N-dimethylformamide)[126] has shown to have a linker based emission at 574 nm under X-ray irradiation. The emission is attributed to intramolecular electron transfer within the linker from carboxylate groups to the central benzene ring. This electron transfer leads to formation of 2-MTA^{2-} radicals which are stabilized and accumulated within the conjugated framework and leads to the observed emission. Benzene derivatives incorporated in the pores of MOFs also help in fine-tuning the emission and conducting properties of the MOFs.

As a result of responsive behaviour towards ionizing radiations, MOFs have found wide applications in X-ray dosimetry, X-ray imagining and X-ray therapy. [118] In addition, because of their responsive behaviour to radiation, MOFs have also found interesting applications in sensing and detection of noble radioactive gases at very low concentrations. Mauree et al.[127] have investigated Zn based photoluminescent MOFs (MOF-5, MOF-9, MOF-205 and MOF-5ADC) to on-line detect the noble radioactive gases. Out of these four MOFs, MOF-205 and MOF-5 outperformed other MOFs for the detection of noble radioactive gases. Using these MOFs as scintillating materials, ^{85}Kr could be concentrated and detected efficiently. In comparison with already existing technologies for online monitoring, it was shown that MOF-205 based scintillation system can be made portable with acceptable detection limit. Using MOF-205 based scintillation, half-life of ^{222}Rn could be determined as 3.7995 days by capturing it within the porous network of MOF-205. Tritiated dihydrogen was also detected using this MOF based scintialltor which is otherwise very difficult to detect using these existing technologies.

Orfano et al.[128] have synthesized hafnium-based MOF incorporating dicarboxy-9,10-diphenylanthracene linkers which act as a scintillating conjugated agents for detecting the radioactive gases (Figure 10). With gas adsorption measurements under varying conditions of temperature and pressure similar to ones existing for the detection of radioactive gases in off-streams of the processing plants, high uptake capacities was observed for Xe and Kr. The Hf-based MOF shows a long lifetime of 2.8 ns with high photoluminescence quantum yield of 0.41 ± 0.06. Using a time coincidence technique, radioactive gases like ^{3}H (low energy β emitter), ^{85}Kr (high energy beta emitter) and ^{222}Rn (α/β emitter) could be efficiently detected on-line through gas flow. A linear response was observed for the detection of ^{85}Kr up to a level of 1 $kBqm^{-3}$ which is the best performance among the existing materials.

Figure 10. *(a) Schematic representation of the fluorescence emission mechanism in Hf-based MOFs. (b) Schematic of triple coincidence system used for the measurements [128].*

7. Conclusions

MOFs can be designed with well defined pore network having particular pore aperture size and open metal sites which effectively determine their capture capacity of noble gases. The uptake capacity and separation selectivity have been increased multifold by screening large number of MOFs through theoretical simulations before selecting a MOF for the noble gas capture. Incorporating the fluorescent properties, MOFs have also shown potential applications for sensing and detecting the noble gases at very dilute concentrations. Tremendous progress has been made in the last decade for enhancement of uptake capacity of noble gases by radiation resistant MOFs. Looking at the MOFs potential for noble gas capture, it is likely that MOFs will play a deterministic role in noble gas capture and separation from the off-stream gases of nuclear reprocessing plants in coming years.

References

1. H. Li et al., Nature, **1999**, 402, 276−279.
2. O. M. Yaghi et al., Nature, **1995**, 378, 703−706.
3. H.-C. Zhou et al., Chem. Rev., **2012**, 112, 673−674.
4. J.-R. Li et al., Chem. Rev., **2012**, 112, 869–932.
5. M. Eddaoudi et al., Science, **2002**, 295 (5554), 469-472.
6. K. S. Park et al., PNAS, **2006**, 103, 10186−10191.
7. C. Janiak et al., New J. Chem., **2010**, 34, 2366–2388.
8. F. Millange et al., Chem. Commun., **2002**, 822–823.
9. S. Noro et al., Nat. Commun., **201**5, 6, 5851.

10. J. H. Cavka et al., J. Am. Chem. Soc., **2008**, 130, 13850–13851.
11. O. V. Gutov et al., Chem. Eur. J., **2014**, 20, 12389 – 12393.
12. J. S. Seo et al., Nature, **2000**, 404, 982-986.
13. R. Grunker et al., Chem. Commun., **2014**, 50, 3450–3452.
14. S. Yang et al., Nature Chemistry, **2012**, 4, 887–894.
15. S. S.-Y. Chui et al., Science, **1999**, 283, 1148–1150.
16. T. Ahnfeldt et al., Angew. Chem. Int. Ed., **2009**, 48, 5163–5166.
17. D. J. David et al., Tetrahedron, **2008**, 64, 8553–8557.
18. O. J. D. L.Neto et al., New J. Chem., **2019**, 43, 5518–5524.
19. J. Klinowoski et al., Dalton Trans., **2011**, 40, 321–330.
20. F. Millange et al., Angew. Chem., **2010**, 122, 775 –778.
21. M. Kalimakow et al., Chem. Mater., **2010**, 22, 5216–5221.
22. W.-J. Son et al., Chem. Commun., **2008**, 6336–6338.
23. C. J. King, Separation Progress, McGraw-Hill, New York, 2nd edn, **1980**.
24. R. T. Yang, Adsorbents: Fundamentals and Applications, John Wiley & Sons, Hoboken, **2003**.
25. B. L. Karger, R. L. Snyder and H. Horvath, An Introduction to Separation Science, Wiley, New York, **1973**.
26. R. Xu, W. Pang, J. Yu, Q. Huo and J. Chen, Chemistry of Zeolites and Related Porous Materials: Synthesis and Structure, John Wiley & Sons (Asia) Pet Ltd., Singapore, **2007**.
27. R. T. Yang, Gas Separation by Adsorption Progress, Butterworth, Boston, **198**7.
28. F. Rouquerol, I. Rouquerol and K. Sing, Adsorption by Powders and Porous Solids-Principles Methodology and Applications, Academic Press, London, **1999**.
29. J. Seader and M. Henley, Separation Process Principles, Wiley, New York, **1998**.
30. D. D. Duong, Adsorption Analysis: Equilibria and Kinetics, Imperial College Press, London, **1998**.
31. S. M. Auerbach, K. A. Carrado and P. K. Dutta, Handbook of Zeolite Science and Technology, Marcel Dekker, Inc., New York, **2003**.
32. D. W. Beck, Zeolite Molecular Sieves, John Wiley & Sons, New York, **1974**.
33. P. A. Warrendale, Nanoporous and Nanostructured Materials for Catalysis Sensor and Gas Separation Applications, Materials Research Society, San Francisco, **2005**.
34. J. M. Loureiro and M. T. Kartel, Combined and Hybrid Adsorbents: Fundamentals and Applications, Springer, Netherlands, **2006**.
35. F. Schuth, K. S. W. Sing and J. Weitkamp, Handbook of Porous Solids, Wiley-VCH, New York, **2002**.
36. J.-R. et al., Chem. Soc. Rev., **2009**, 38, 1477–1504.
37. C. Sanchez et al., J. Mater. Chem., **2005**, 15, 3559–3592.
38. B. Moulton and M. J. Zaworotko, Chem. Rev., **2001**, 101, 1629–1658.
39. M. J. Zaworotko, Chem. Commun., **2001**, 1–9.
40. O. R. Evans and W. Lin, Acc. Chem. Res., **2002**, 35, 511–522.
41. M. J. Rosseinsky, Microporous Mesoporous Mater., **2004**, 73, 15–30.
42. G. S. Papaefstathiou and L. R. MacGillivray, Coord. Chem. Rev., **2003**, 246, 169–184.
43. L. Brammer, Chem. Soc. Rev., **2004**, 33, 476–489.
44. R. J. Hil et al., Acc. Chem. Res., **2005**, 38, 335–348.
45. S. Kitagawa et al. Chem. Commun., **2006**, 701–707.
46. M. Hong, Cryst. Growth. Des., **2007**, 7, 10–14.
47. M. Dincă and J. R. Long, J. Am. Chem. Soc., **2005**, 127, 9376–9377.
48. S. Q. Ma et al., Inorg. Chem., **2007**, 46, 8499–8501.
49. C.-J. Li et al., Chem. Commun., **2008**, 6348–6350.
50. J. A. R. Navarro et al., J. Am. Chem. Soc., **2008**, 130, 3978–3984.
51. M. Xue et al., Inorg. Chem., **2008**, 47, 6825–6828.
52. J.-R. Li et al., Chem.–Eur. J., 2008, 14, 2771–2776.
53. R. Matsuda et al., Nature, **2005**, 436, 238–241.
54. L. Pan et al., Angew. Chem., Int. Ed., **2006**, 45, 616–619.
55. L. Pan et al., J. Am. Chem. Soc., **2006**, 128, 4180–4181.
56. J. Y. Lee et al., Adv. Funct. Mater., **2007**, 17, 1255–1262.
57. Y.-S. Bae et al., Langmuir, **2008**, 24, 8592–8598.
58. H. R. Moon et al., Inorg. Chem., **200**6, 45, 8672–8676.
59. T. K. Maji et al., Angew. Chem., Int. Ed., **2004**, 43, 3269–3272.
60. Y. E. Cheon and M. P. Suh, Chem.–Eur. J., **2008**, 14, 3961–3967.
61. M. J. Lee et al., Angew. Chem., Int. Ed., **2018**, 57, 156−161.
62. Q. Hou et al., J. Am. Chem. Soc., **2020**, 142, 9582−9586.
63. A. Knebel et al.. Science, **2017**, 358, 347−351.
64. P. Krokidas et al., J.Phys. Chem. C, **2016**, 120, 8116−8124.
65. C. Wang, et al., Chem. Commun., **2016**, 52, 12578−12581.
66. A. Knebel et al., Chem. - Eur. J., 2018, 24, 5728.
67. S. Bourrelly et al., J. Am. Chem. Soc., **2005**, 127, 13519–13521
68. H. Hayashi et al., Nat. Mater., **2007**, 6, 501–506.
69. R. Kitaura et al., Angew. Chem., Int. Ed**., 2003**, 42, 428–431.
70. C. L. Hobday et al., Nat. Commun**., 2018**, 9, 1429.
71. D. Fairen-Jimenez et al., J. Am. Chem. Soc., **2011**, 133, 8900−8902.
72. P. Zhao et al., Chem. Mater**., 2014**, 26, 1767−1769.
73. P. Zhao et al. Nature Commun., **2019**, 10, 999.
74. Du, Y. et al., J. Am. Chem. Soc., **2015**, 137, 13603−13611.
75. J. Mor et al., J. Phys. Chem. C, **2023**, 127, 2160−2172.
76. J. Mor et al., J. Phys. Chem. C, **2024**, 128, 6496−6502.
77. P. K. Thallapally et al., Chem. Commun., **2012**, 48, 347−349.
78. Kerry, F. G. Industrial Gas Handbook: Gas Separation and Purification; CRC Press: Boca Raton, FL, **2007**.
79. Soelberg, N. R. et al., Sci. Technol. Nucl. Install. **2013**, No. 702496.
80. Little, D. K. Eby, R. S.Norton, J. L.Patton, J. L.Schultz, R. M.Varagona, J. M. Noble Gas Removal and Concentration by Combining Fluorocarbon Absorption and Adsorption Techniques; Oak Ridge Gaseous Diffusion Plant: Oak Ridge, TN, **1982**.
81. Separation, Storage and Disposal of Krypton-85; International Atomic Energy Agency: Vienna, **1980**.
82. C. J. Jameson et al., J. Chem. Phys., **1997**, 107, 4364−4372.
83. R. E. Bazan et al., Adsorption, **2011**, 17, 371−383.

84. D. Banerjee et al., Acc. Chem. Res., **2015**, 48, 211−219.
85. IAEA Annual Report-Activities of the President of the National Atomic Energy Agency and Assessment of Nuclear Safety and Radiological Protection in Poland in 2018; IAEA**, 2019**.
86. IAEA, ILO Radiation Protection against Radon in Workplaces other than Mines; IAEA, **200**3.
87. Y. Nakano et al., Phys. Res., Sect. A, **2017**, 867, 108– 114.
88. U. Mueller et al., J. Mater. Chem. **2006**, 16, 626−636.
89. Z. Hulvey et al., J. Phys. Chem. C, **2013**, 117, 20116−20126.
90. J. Liu et al., Langmuir, **2012**, 28, 11584−11589.
91. W. Bohlmann et al., J. Phys. Chem. B, **2006**, 110, 20177−2018.
92. P. Ryan et al., AIChE J. **2011**, 57, 1759−1766.
93. B. J. Sikora et al., Chem. Sci., **2012**, 3, 2217−2223.
94. S. R. Caskey et al., J. Am. Chem. Soc., **2008**, 130, 10870− 10871.
95. J. J. Perry et al., J. Phys. Chem. C, **2014**, 118, 11685−11698.
96. J. Liu et al., Chem. Commun., **2014**, 50, 466−468.
97. J. Liu et al., Ind. Eng. Chem. Res., **2014**, 53, 12893− 12899.
98. H. Wang et al., Chem. Sci., **2014**, 5, 620−624.
99. K. V. Lawler et al., Chem. Commun., **2013**, 49, 10959−10961.
100. Y. S. Bae et al., Microporous Mesoporous Mater., **2013**, 169, 176−179.
101. S. Xiong et al., J. Mater. Chem. A, **2018**, 6, 4752.
102. S.-J. Lee et al., J. Hazard. Mater., **2016**, 320 513–520;
103. Z. Niu et al., Angew. Chem. **2022**, 134, e202117807.
104. X. Chen et al., J. Am. Chem. Soc., **2015**, 137, 7007−7010.
105. D. Banerjee et al., Nat. Commun., **2016**, 7, 11831.
106. Q. Liu et al., J. Chem. Eng., **2023**, 453, 139849.
107. T. Hurley et al., ACS Appl. Mater. Interfaces, **2024**, 16, 35333−35341.
108. K. B. Idrees et al., Chem. Mater., **2020**, 32, 3776−3782.
109. S. T. Meek et al., J. Phys. Chem. C, **2012**, 116, 19765−19772,
110. Y. Gong et al., J. Mater. Chem. A, **2018**, 6, 13696.
111. J. Pei et al., J. Am. Chem. Soc., **2022**, 144, 3200−3209.
112. J. J. Perry et al., J. Phys. Chem. C, **2014**, 118, 11685−11698.
113. X.-L. Wu et al., Inorg. Chem., **2021**, 60, 1506−1512.
114. Z. Yan et al., Cryst. Growth Des., **2020**, 20, 8039−8046.
115. X. Wang et al., J. Am. Chem. Soc., **2022**, 144, 13634−13642.
116. X. Zeng et al., J. Hazard. Materi., **2019**, 366 624–629.
117. W. Park et al., J. Chem. Eng., **2023**, 452, 139189.
118. Chen et al. Adv. Funct. Mater., **2024**, 34, 2310270.
119. L. S. Xie et al., Chem. Rev., **2020**, 120, 8536.
120. Z. Li et al., Nano Lett., **2021**, 21, 6983.
121. Y.-F. Han et al., Chem. Eng. J., **2022**, 437, 135468.
122. L. Pu, Chem. Rev., **2004**, 104, 1687.
123. B. Zheng et al., Chem. Rev., **2022**, 122, 5519.
124. T.-W. Duan and B. Yan, J. Mater. Chem. C, **2014**, 2, 5098.
125. Q. Yao et al., Chem. Mater., **2015**, 27, 5332.
126. H. Liu et al., Angew. Chem. Int. Ed., **2020**, 59, 15209.
127. S. Mauree et al., Adv. Funct. Mater., **2023**, 33, 2302877.
128. M. Orfano et al., Nature Photonics, **2023**, 17, 672–678.

Dr. Sandeep K Sharma *joined Radiochemistry Division, BARC in 2006 after graduating from the 49th batch of training school. He obtained his PhD from Homi Bhabha National Institute, Mumbai in 2012. His research work is primarily focused on application of positron annihilation spectroscopy for the characterization of advanced materials. He is recipient of Indo-French PhD fellowship-2008, Indo-US postdoc fellowship-2013, HBNI outstanding thesis award-2015, DAE Young Scientist Award-2014 and DAE S&T excellence Award-2019. He has published 110 research papers in peer reviewed international journals.*

Mr. Jaideep Mor *joined the Radiochemistry Division, BARC in 2020. Currently, his research focuses on the fundamental study of porosity and flexibility of Metal Organic Frameworks (MOFs) using Positron annihilation spectroscopy and other complementary techniques. In terms of applications, he is investigating the potential of MOFs in areas such as catalysis, supercapacitor, polymer nanocomposites, and adsorption of f-block elements. He has around 25 publications in peer reviewed international journals.*

Sulphur-Ligand Functionalized MOFs as Highly Efficient Adsorbents for Aqueous Mercury ions

A. K. Singha Deb[1], S. Kolay[2], Manju Mohan[1], Sk. Musharaf Ali[1,3]
[1]*Chemical Engineering Division, Bhabha Atomic Research Centre, Trombay, Mumbai – 400 085*
[2]*Chemistry Division, Bhabha Atomic Research Centre, Trombay, Mumbai – 400 085*
[3]*Homi Bhabha National Institute, Anushaktinagar, Mumbai – 400 094*

Abstract

Due to the highly solubility in the aquatic environments associated with chronic toxicity of heavy metal ions, such as, Hg^{2+}, it can be absorbed easily by living organisms causing harmful effects. This necessitates decontamination of water from these toxic metal ions. Here, sulphur ligands were functionalized into metal organic framework adsorbents to increase their effectiveness in removing mercury ions, allowing them to decontaminate water with extremely low concentrations of mercury ions. Thiol (SH) and xanthic acid (OCS_2H) ligands were functionalized on to the surface of MIL-199 (Cu) and MOF-74 (Ni) pristine metal organic frame works, respectively. The structure and functional groups of the prepared pristine and functionalized MOFs were analyzed by using AAS, XRD and FTIR techniques. Batch adsorption of mercury ions by the prepared materials revealed that MOF-74 showed higher adsorption capacity than MIL-199 due to the presence of hydroxyl groups in the linker unit. xanthic acid functionalized MOF-74 (MOF-74-OCS_2H) showed better performance than thiol functionalized MIL-199 (MIL-199-SH). Various adsorption parameters were optimized. Adsorption equilibrium experiments revealed that Langmuir isotherm model best fitted with the data showing adsorption capacities of MIL-199-SH and MOF-74-OCS_2H as 333 and 840 mg/g at pH 4 and room temperature. This study provide a possible strategy to design sulphur ligand functionalized MOF based adsorbents for removal of mercury ions from waste effluent stream.

1. Introduction

Rapid industrialization has exacerbated the problem of availability of fresh and clean water as it has been accompanied with a large number of toxic heavy metals being discharged into the environment in industrial wastewater over the past few years [1, 2]. Mercury (Hg) is one such non-biodegradable heavy metal, for which the recent estimations suggest global anthropogenic releases to be 1000 tonnes a year [2]. It has been categorized as a "priority hazard substance" by the Agency for Toxic Substances and Disease Registry (ATSDR) because of its toxicity, mobility and a long residence time in the atmosphere [3]. The appalling Minamata disease discovered in 1956 in Minamata city of Japan was a result of mercury poisoning caused by eating seafood contaminated with methyl mercury that was discharged into Minamata Bay through industrial wastewater [4]. Mercury poisoning severely impairs neurological development and pulmonary function, causes blindness, paralysis, and can even cause breakage of chromosomes [5, 6]. The most common form in which it exists is Hg(II), which readily binds to organic and inorganic matter, thereby posing a threat to aquatic life while also rendering the water unfit for public use [1, 7].

In spite of its extraordinarily poisonous nature, mercury is utilized mainly in the chlor-alkali, oil refinery, metal finishing, fertilizer, chemical, mining, smelting, power generation, paper, pulp, and rubber processing industries [8 - 11]. Mercury is also used in wide range of consumer products, including dental amalgams, batteries, electronic devices, blood-pressure gauges, thermometers, fluorescent and energy-saving lamps, pesticides, fungicides, cosmetics and medicines [12, 13]. Once used, many of these products and the mercury enter the wastewater directly or leach into water from disposal sites [13]. As per the US Environmental Protection Agency, the tolerance limit of mercury in drinking water is 2 µg/L ppm [14], while the World Health Organization (WHO) and the Bureau of Indian Standards (BIS) have set the permissible limit to 2 µg/L [15, 16]. The discharge limit of mercury in industrial wastewater is 10 µg/L as per Central Pollution Control Board, India. Mercury-containing wastewater must therefore be treated before being released into the receiving environment in order to reduce its serious effects.

Owing to this, number of separation techniques have been developed for removal of mercury from wastewater. Amongst various processes that have been used such as solvent extraction [17], ion-exchange [18], membrane filtration [19, 20], electrochemical reduction, precipitation,

and electro dialysis [21-24], adsorption based processes offers significant advantages in many aspects such as generation of minimum amount of secondary waste, easy operation and possibility to achieve very low TLV values. That is why, adsorption based separation technologies either as sole process or as in combination with other different processes has now become one of the most commonly used methods, due to its simplicity, effectiveness, ease of operation and reusability [25, 26]. Adsorption process is determined mainly by the properties of the adsorbents. Conventional adsorbents such as resins, activated carbon, mesoporous carbon, silica and biosorbents have been utilized for mercury removal from aqueous solution. These adsorbents have limited adsorption capacity and selectivity for mercury and hence the desired TLV concentration may not be achieved by these materials. With the advent of nanotechnology, various porous nanomaterial based adsorbents, bearing high surface area and high reactivity, have been shown to possess better mercury adsorption behaviours. Recently a new class of porous materials, Metal organic framework (MOFs) are an emerging as nano-adsorbent for environmental remediation technologies [27]. The MOF is an organic-inorganic polymeric framework material formed by coordination of metal ions or metal clusters with organic ligands or linkers. The main features that makes MOF a good absorbent include large specific surface area, designable frame structure, controllable pore size, metal unsaturation sites, easy to modify etc. Over the past two decades, several hundred different MOFs have been studied for different applications, including gas separation, gas storage, sensing, photocatalysis, drug loading, and environmental applications [28-40].

Removal of heavy metal ions from effluent stream using highly porous and tunable microstructure MOFs, is one of its primary application as reported in various literature [41-45]. Among heavy metals, mercury, a soft B-group metal, exhibits relatively weak interactions with oxygen containing ligands, moderate strength interactions with nitrogen-containing ligands, and strong interactions with sulfur-containing ligands [46]. Thus sensitivity and selectivity of MOFs towards mercury adsorption can be enhanced by modifying its surface by sulphur containing ligands such as thiol, dithiocarbamate, xanthic acid, etc. Increase in the adsorption efficiency of carbon nanotubes by introduction of such functional groups has been reported [47]

Owing to this, here thiol (SH) and xanthic acid (OCS_2H) ligands were functionalized on to the surface of MIL-199 (Cu) and MOF-74 (Ni) pristine metal organic frame works, respectively. The Hg^{2+} ions adsorption by these two S-ligand functionalized MOFs from aqueous solution were investigated by batch method. The performances of both the base MOFs as well as functionalized MOFs was compared by carrying out adsorption experiments varying various parameters.

2. Preparation of sulphur-Ligand Functionalized MOFs

Solvothermal methods were used to synthesize the base MOFs (MIL-199 and Ni-MOF-74) which were then functionalized with sulphur ligands (thiol and xanthate, respectively) using post synthetic modification protocol [48].

2.1 Synthesis and characterization of thiol functionalized MIL-199 (MOF-199-SH)

First MIL-199 was synthesized according to available literature methods [49-51]. In a typical preparation, a solid mixture of $Cu(NO_3)_2 \cdot 3H_2O$ and 1,3,5-benzenetricarboxylic acid was dissolved in a mixture of DMF, ethanol and water in a 100 ml Teflon-lined autoclave vial. The vial was heated at 85°C inside an oven for 24 h, yielding light blue crystals. After cooling the vial to room temperature, the solid product was obtained by decanting with mother liquor and washed 3-4 times with DMF through centrifugation in centrifuge tubes. Solvent exchange was then carried out 3-4 times with ethanol through centrifugation in centrifuge tubes at room temperature. The product was then dried under vacuum at 170°C for overnight, yielding MIL-199 in the form of deep purple crystals.

In the post synthetic modification step, the prepared MIL-199 was dispersed in toluene under ultrasonic agitation followed by stirring at room temperature. 1,2-Ethanedithiol was added into the suspension and agitated for 24 hours at room temperature. After the reaction, the solid product was separated from the mixture by centrifugation, washed with toluene followed by ethanol and the dried at 85°C in vacuum oven for overnight. A schematic of the synthetic route is shown in Fig. 1.

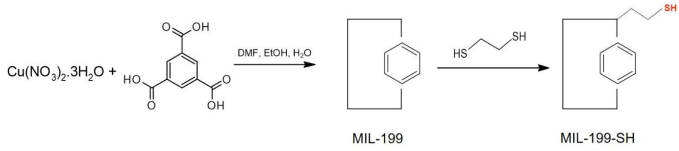

Fig. 1. Schematic reactions steps for the synthesis of MIL-199-SH

The prepared materials, the base MOF, MIL-199 as well as the thiolated MOF, MIL-199-SH were characterized by XRD and FTIR analysis. Elemental atomic absorption spectroscopic (AAS) analysis confirmed the loading of Cu in the MOF phase ~5 mmol/g. Powder XRD investigation

verified the MIL-199's crystalline phase purity. (Fig. 2a). The diffraction peaks of the MIL-199 were consistent with the simulated patterns from the single crystal data as shown in Fig. 2a, and with those reported in the literature [52]. That the crystal structure of the base MOF has been retained after post synthetic fuctionalzion is clear from the similar XRD pattern of MIL-199-SH as shown in Fig. 2a. The FTIR spectra of base and functionalized MOFs are shown in Fig. 2b. The appearance of strong peaks at 1630 cm^{-1} in conjunction with the less strong absorption bands at 1760–1690 cm^{-1} confirmed the deprotonation of –COOH groups in 1,3,5-benzenetricarboxylic acid upon the reaction with copper ions. The feature of IR spetra of both the MOFs are is almost similar. The IR spectrum of MIL-199-SH showed an extra peak at 682cm^{-1} which can be attributed to the C-S bond frequency. This confirms the covalent linking of ethanedithiol in the structure of MIL-199.

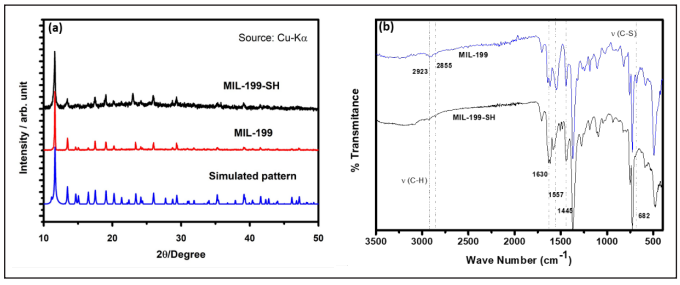

Fig. 2. XRD pattern (a) and FTIR spectra (b) of MIL-199 before and after thiolation reaction

2.2 Synthesis and characterization of xanthate functionalized Ni-MOF-74 (Ni-MOF-74-OCS_2)

Ni-MOF-74 was first synthesized by solvothermal method as described by Y. Guo et al. [53]. Briefly, $Ni(NO_3)_2 \cdot 6H_2O$ and 2,5-Dihydroxy-1,4-benzenedicarboxylic acid (DHDBC) was dissolved in a solution composed of DMF, EtOH and H_2O mixture with a volume ratio of 1:1:1 and placed in an ultrasonic bath. Next, the mixture was transferred into a 250mL teflon-lined hydrothermal autoclave reactor and heated at 100°C for 24h. The fine yellow crystalline product formed (nickel-2,5-dihydroxy-1,4-dicarboxylate, Ni-MOF-74) was collected by centrifugation and washed several times with EtOH, MeOH and H_2O, successively. Finally, the product was dried under the vacuum at 150°C overnight.

In post synthetic reaction, MOF-74 was dispersed into sodium hydroxide solution to obtain the stable suspension with stirring and ultrasonication. The mixture was stirred overnight and stirred magnetically at 95 °C in an oil bath for 3 h. Then the mixture was cooled to room temperature and added dropwise 5 mL ethyl alcohol and 5 mL carbon disulfide (CS_2) followed by stirring the mixture for 12h. The mixture was allowed to stand and the reddish supernatant solution was decanted. The residue was purified by repeated centrifugation washing with acetone, ethyl alcohol, methyl alcohol and deionized water, successively. Finally, the product (MOF-74-OCS_2H) was transferred into a Petri dish and dried in a vacuum oven at 50°C for 24h. A schematic of the reaction is shown in Fig. 3.

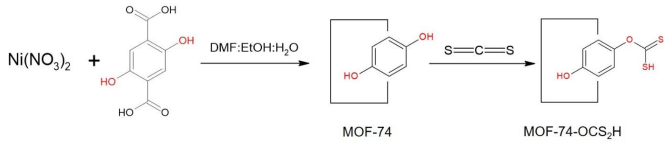

Fig. 3. Schematic reactions steps for the synthesis of MIL-199-SH

The formation of Ni-MOF-74 crystal structure by the Solvothermal reaction of nickel ions and DHDBC is confirmed by XRD. The XRD pattern of MOF-74-OCS_2H is consistent with the simulation XRD pattern of MOF-74 reported in the literature as shown in Fig. 4a [53, 54]. The XRD pattern of the prepared MOF-74 in Fig. 4a reveals the peaks at 6.84°, 11.88°, 24.92°, 33.74°, and 36.34°, which are in good agreement with reported MOF-74 [55].

FTIR spectra of Ni-MOF-74 and its xanthate derivative are shown in Fig. 4b. In the MOF-74 spectrum, the characteristic peaks at around 1558, 1419 cm^{-1} are ascribed to stretching vibrations of symmetric and asymmetric carboxylate groups (–COO–). Moreover, the peaks are located at 920, 850, and 3415 cm^{-1}, which are attributed to stretching vibration of Ni–O, C–H, and –OH bonds, respectively. The IR spectrum of MOF-74-OCS_2H resembles almost with the spectrum of base MOF except two major changes. Absorption peaks appeared around 1020 cm^{-1} of MOF-74-OCS_2H corresponding to the C=S stretching vibration of the xanthate unit and the diminution of the hydroxyl peak (1370 cm^{-1}) after xanthation was strongly indicative of the presence of xanthate group bonded to the charred materials.

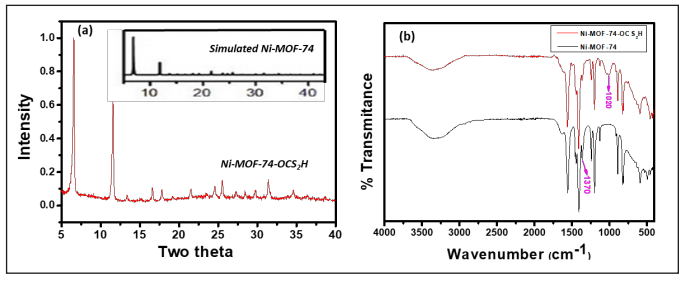

Fig. 4. XRD pattern (a) and FTIR spectra (b) of MOF-74 before and after xanthation reaction

3. Evaluation of Hg^{2+} removal efficiency in aqueous medium

In view of the practical application of adsorption, the divalent mercury ions, Hg^{2+}, adsorption behavior of

the prepared base MOFs (Cu-MIL-199 and Ni-MOF-74) and sulphur-ligand functionalized MOFs (MIL-199-SH and MOF-74-OCS_2H) materials were evaluated using adsorption theory. This theory [relates the dependences of the adsorbed amount on the characteristic process parameters on a theoretical basis. Initially physical parameters such as temperature, pH and time of agitation are optimized in batch adsorption studies. The practice-oriented adsorption theory consists of three main elements: the adsorption equilibrium, the adsorption kinetics, and the adsorption dynamics. The adsorption equilibrium describes the dependence of the adsorbed amount on the adsorbate concentration and the temperature. The primary components of the practice-oriented adsorption theory are depicted in Fig. 5, along with their interdependencies. The q, c, t, and z denotes adsorption capacity of adsorbent, concentration of adsorbate, time of adsorption, and spatial length, respectively. All adsorption models are based on the adsorption equilibrium. The use of both kinetic and dynamic adsorption models requires an understanding of the adsorption equilibrium. Both adsorption equilibrium and adsorption kinetics data are required to forecast adsorption dynamics.

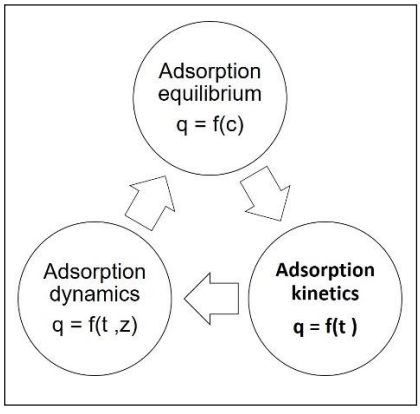

Fig. 5. Elements of the adsorption theory.

The materials were subjected for adsorption of mercury ions from aqueous solution through optimization of pH for optimum adsorption efficiency followed by adsorption equilibrium data generation in the proceeding sections.

3.1 Adsorption of Hg^{2+} by MIL-199 and MIL-199-SH

The pH of any solution plays a significant role in determining the adsorption of metal ions from it. In order to determine the effect of pH on the adsorption of mercury ions by the prepared MIL-199 and MOF-199-SH, experiments were carried out using solutions having the varying pH values from 2 to 12, while keeping all the other parameters, such as temperature, feed volume, feed concentration, etc. constant. As shown in Fig. 6a, pH do not have any significant effect for adsorption capacity (q_e) by MIL-199, whereas for MIL-199-SH it has a unique dependence. The Hg^{2+} adsorption initially increases from pH 2 to 5, decreases from pH 5 to 7, again increases from pH 7 to 10 and after which it can be seen to decrease again. The adsorption capacity of MIL-199-SH has more than three time higher adsorption efficiency compared to the pristine MOF-199. The clear role of thiol groups in binding the mercury ions is seen from this enhancement in adsorption capacity. From the experimentally observed data, it can be concluded that at a low pH, that is, for pH<5, there is competition between Hg^{2+} ions and H^+ ions in the solution, which leads to a decrease in the amount of Hg^+ ions adsorbed. The presence of negatively charged species of mercury such as $HgCl_3^-$, $Hg(OH)_3^-$, $HgCl_4^{2-}$ exist at the higher pH range [57], may be responsible for the decline in adsorption capacity as negatively charged thiol binding sites would repeal these forms of mercury. The increase of capacity in the range of pH 7 to 10, may be due to the appearance of another cationic species, $Hg(OH)^+$ in the solution [57]. The optimum pH of the metal ion solution used for further studies was decided to be 4 to 5 and further experimentations were conducted at this optimum pH.

The equilibrium data for the Hg^{2+}adsorption by MIL-199 and MOF-199-SH was generated by varying initial feed mercury concentration from 10 to 1800 mg/L at room temperature, pH 4 and 1 mg/mL adsorbent dose. The extent of adsorption increases with increase in feed mercury concentration, showed maximum at 1500 mg/L and then decreases. The maximum adsorption capacity showed by MIL-199 and MIL-199-SH are 217 and 333 mg/g. Adsorption data were fitted to Langmuir and Freundlich isotherm model showing better fit to the former one indicating chemical adsorption as a prime step during adsorption of the Hg2+ ions on the MOF adsorbent. This reflects that surface complexation of the metal ions with the thiol or xanthic acid occurred during adsorption process.

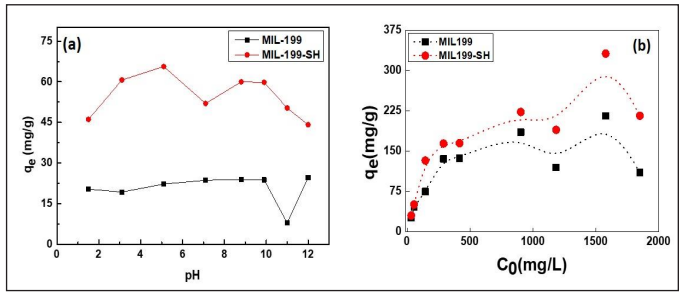

Fig. 6. Batch adsorption of Hg^{2+} ions by MIL-199 and MIL-199-SH: effect of pH (a) and feed concentration (b)

3.2 Adsorption of Hg^{2+} by Ni-MOF-74 and MOF-74-OCS_2H

The solution pH has a great effect on the adsorption of the metal ions by the adsorbent. In this experiment, extent of adsorption was tested between pH 2 and 10 keeping feed concentration and adsorbent dosages a fixed value. A strong dependence of equilibrium adsorption capacity (q_e) on the pH was observed as shown in Fig. 7a. When the solution pH was low, it was observed that the adsorption capacity was as low as 77.99 mg/g, while at higher pH it reduced to 83.04 mg/g. The optimal conditions for the adsorption of Hg^{2+} ions by MOF-74-OCS_2H was found at pH 4. At lower pH, there is competition between the H^+ and Hg^{2+} ions to bind at the xanthate group which lowers the adsorption. On the other side, when pH > 4, depending on the amount of hydroxyl and chloride ions, different species such as $Hg(OH)_2$, $Hg(OH)^+$, Hg(OH)Cl, etc. were formed in the resultant solution effecting the adsorption capacity. Hence, an optimum pH at 4 was chosen in carrying out other separation experiments.

The dependence of adsorption capacity of the adsorbent, MOF-74-OCS_2H, on the initial feed concentration of mercury ions in the fluid phase was shown in Fig. 7b. The initial feed mercury ion concentration was varied from 10 to 10000 mg/L at room temperature, pH 4 and adsorbent dosages of 1mg/mL. The adsorption capacity of MOF-74-OCS_2H for Hg^{2+} ions increases with increasing the concentration of Hg^{2+} ions if feed solution and it reaches equilibrium after 4000 mg/L Hg^{2+} concentration. Once all the binding sites (mainly xanthic acids) of the adsorbent covered by the adsorbate Hg^{2+} ions at higher feed concentration, adsorption capacity reaches a plateau indicating attainment of equilibrium. The linear plot of specific adsorption (C_e/q_e) against the equilibrium concentration (C_e) showed that the adsorption of Hg^{2+} ions on the surface of MOF-74-OCS_2H obeys the Langmuir isotherm model with maximum monolayer adsorption capacity of 840 mg/g. The applicability of Langmuir model for the description of equilibrium data also reflects that adsorption of Hg^{2+} ions on MOF-74-OCS_2H is a chemisorption phenomenon where metal ions coordinate with the xanthic acid binding sites.

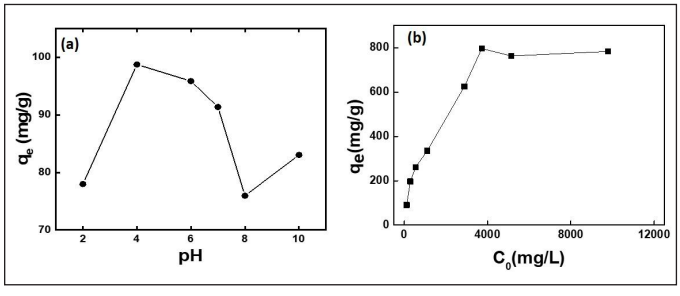

Fig. 7. Batch adsorption of Hg^{2+} ions by MOF-74-OCS_2H: effect of pH (a) and feed concentration (b)

3.3 Comparison of adsorption efficiencies between prepared

Adsorption studies were carried out on 200ppm Hg^{2+} solution (pH 4) by MILL-199, MIL-199-SH, MOF-74 and MOF-74-OCS_2H in order to compare the capacity while realizing the potential of functionalizing MOFs for adsorption process of mercury. Fig. 8 represents the capacities of each of the materials analyzed. It is clearly observed that MOF-74 has higher mercury adsorption that MIL-199 owing to the presence of hydroxyl functional group in the linker which may take part in binding with mercury cation. Again, xanthic acid functionalization enhances the adsorption in higher extent compared to thiolation.

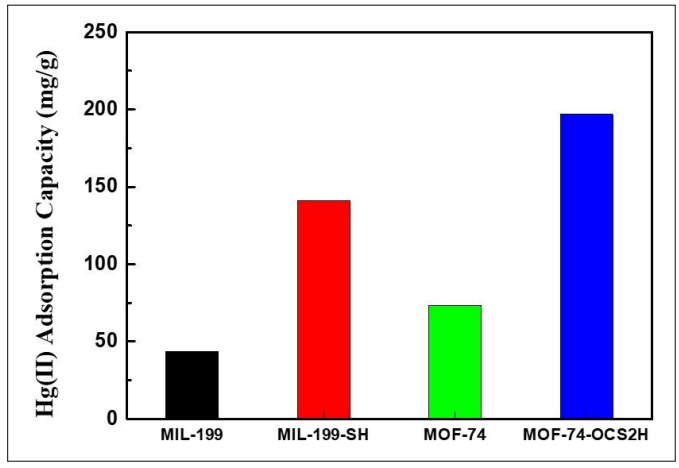

Fig. 8. Adsorption capacities of the prepared pristine-MOFs and S-ligand-modified MOFs

4. Conclusion

After synthesizing two types of base MOFs (MIL-99 and MOF-74), these were functionalized with thiol and xanthic acid ligands, respectively, containing sulphur binding sites to improve the Hg^{2+} adsorption capability. The prepared functionalized MOFs retained the crystal phases after post synthetic modification reaction as confirmed from XRD and FTIR analysis. FTIR spectral data were used to confirm the introduction of S-ligands of the MOF. The prepared functionalized MOFs were then tested for Hg^{2+} uptake from aqueous solution in varied experimental conditions. Adsorption capacity have seen to increased 3 to 4 times after the functionalization for both of the MOFs. Highest adsorption capacities of MIL-199-SH and MOF-74-OCS_2H observed as 333 and 840 mg/g at pH 4 and room temperature. Adsorption equilibrium data were used to understand the mechanism of the interaction

between Hg^{2+} and MOF adsorbent and to find out the maximum adsorption capacity. This study had shown that suitable functionalization of MOFs can be followed to enhance the sensitivity of the adsorbent towards mercury removal from aqueous system. The same strategy can be utilize to design new MOF based adsorbents for treatment of waste water for removal of toxic heavy metal ions.

Acknowledgement

The authors acknowledge Shri K. T. Shenoy, Director ChEG, BARC and Dr. Sulekha Mukhyopadhyay, Head, ChED, BARC for encouragement and support.

References

1. Rongjun Q.; Wang, M.; Song, R.; Sun, C.; Zhang, Y.; Sun, X.; Ji, C.; Wang, C.;Yin, P. Adsorption kinetics and isotherms of Ag(I) and Hg(II) onto silica gel with functional groups of hydroxyl- or amino-terminated polyamines. J. Chem. Eng. Data 2011, 56, 1982–1990.
2. UNEP, 2013. Global Mercury Assessment 2013: Sources, Emissions, Releases and Environmental Transport. UNEP Chemicals Branch, Geneva, Switzerland
3. ATSDR, 2015. Summary Data for 2015 Priority List Of Hazardous Substances, Division Of Toxicology & Human Health Sciences, Agency for Toxic Substances and Disease Registry, Atlanta, USA.
4. Ministry of the Environment, 2013. Lessons from Minamata Disease and Mercury Management in Japan, Tokyo, Japan.
5. Namasivayam, C.; Kadirvelu, K. Uptake of Mercury (II) from Waste water by Activated Carbon from an Unwanted Agricultural Solid by-product: Coirpith. Carbon 1999, 37, 79–84.
6. Song, S.T.; Saman, N.; Johari, K.; Mat, H. Removal of Hg(II) from aqueous solution by adsorption using raw and chemically modified rice straw as novel adsorbents. Ind. Eng. Chem. Res. 2013, 52, 13092−13101.
7. Hsiao H.W.; Ullrich S.M.; Tanton T.W. Burdens of mercury in residents of Temirtau, Kazakhstan I: hair mercury concentrations and factors of elevated hair mercury levels. Sci Total Environ. 2011, 409, 2272–2280.
8. Streets, D. G.; Horowitz, H. M.; Jacob, D. J.; Lu, Z.; Levin, L.; ter Schure, A. F. H.; Sunderland, E. M. Total Mercury Released to the Environment by Human Activities Environ. Sci. Technol. 2017, 51, 11, 5969–5977
9. Wankhade, K.K. Mercury in India: Toxic Pathways, Toxic link 2003, New Delhi, India.
10. Wei Yuan, Xun Wang, Che-Jen Lin, Ge Zhang, Fei Wu, Nantao Liu, Longyu Jia, Hui Zhang, Huazheng Lu, Jinlong Dong, Xinbin Feng. Fate and Transport of Mercury through Waterflows in a Tropical Rainforest. Environmental Science & Technology 2024, 58 (11), 4968-4978.
11. Hadavifar, M.; Bahramifar, N.; Younesi, H.; Li, Q. Adsorption of mercury ions from synthetic and real waste water aqueous solution by functionalized multi-walled carbon nanotube with both amino and thiolated groups. Chem. Eng. J. 2014, 237, 217–228.
12. Rhee, S. W. Estimation of mercury amount in the components of spent U-type lamp. Environmental Technology 2017, 38:10, 1305-1312.
13. Beckers, F.; Rinklebe, J. Cycling of mercury in the environment: Sources, fate, and human health implications: A review. Critical Reviews in Environmental Science and Technology 2017, 47(9), 693–794.
14. US EPA, April 2012. 2012 Edition of the Drinking Water Standards and Health Advisories, Washington, USA.
15. WHO 2008. Guidelines for drinking-water quality, Vol. 1, 3rd Ed. World Health Organization, Geneva.
16. Kumar, M.; Puri, A. A review of permissible limits of drinking water. Indian J. Occup. Environ. Med. 2012, 16, 40–44.
17. Rice, N.M.; Smith, M.R. Recovery of Zinc, Cadmium and mercury (II) from chloride and sulphate media by solvent extraction. J. Appl. Chem. Biotechnol. 1975, 25, 379-402.
18. Dąbrowski, A.; Hubicki, Z.; Podkościelny, P.; Robens, E.; Selective removal of the heavy metal ions from waters and industrial wastew aters by ion-exchange method. Chemosphere 2004, 56, 91–106.
19. Meltem Urgun-Demirtas, M; Benda, P. L.; Gillenwater, P. S.; Negri, M. C.; Xiong, H.; Snyder, S. W. Achieving very low mercury levels in refinery wastewater by membrane filtration, Journal of Hazardous Materials 2012, 215–216, 98-107.
20. Barron-Zambrano, J.; Laborie, S.; Viers, P.; Rakib, M.; Durand, G. Mercury removal from aqueous solutions by complexation-ultrafiltration. Desalination 2002, 144, 201–206.
21. Tunsu, C., Wickman, B. Effective removal of mercury from aqueous streams via electrochemical alloy formation on platinum. Nat Commun., 2018, 9, 4876.
22. Bolger, P. T.; Szlag, D. C.; An Electrochemical System for Removing and Recovering Elemental Mercury from a Gas Stream, Environ. Sci. Technol. 2002, 36, 20, 4430–4435.
23. Tami-Pimiento, L.M., Joya-Herrera, L.M., Pérez-Chía, Y.I. et al. Selective electrochemical reduction of mercuryII. from a simulated traditional gold mining wastewater contaminated with cyanide and heavy metals. J Solid State Electrochem. 2024, 28, 2223–2232.
24. Rodríguez O, Padilla I, Tayibi H, López-Delgado A. Concerns on liquid mercury and mercury-containing wastes: a review of the treatment technologies for the safe storage. J. Environ. Manag. 2012;101:197–205.
25. J. G. Yu, B.Y . Yue, X. W. Wu, Q. Liu, F. P. Jiao, X. Y. Jiang, X. Q. Chen, Removal of mercury by adsorption: a review, Environ. Sci. Pollut. Res. 2016, 23, 5056–5076.
26. A. Sharma, A. Sharma, R. K. Arya, Removal of MercuryII. from Aqueous Solution:A Review of Recent Work, Sep. Sci. Technol. 2015, 50, 1310–1320.
27. Lesley Joseph, Byung-Moon Jun, Min Jang, Chang Min Park, Juan C. Muñoz-Senmache, Arturo J. Hernández-Maldonado, Andreas Heyden, Miao Yu, Yeomin Yoon, Removal of contaminants of emerging concern by metal-organic framework nanoadsorbents: A review, Chemical Engineering Journal, 2019, 369, 928-946.
28. H. Furukawa, K.E. Cordova, M. O'Keeffe, O.M. Yaghi, The chemistry and applications of metal-organic frameworks, Science 2013, 341, 1230444.

29. M. Eddaoudi, J. Kim, N. Rosi, D. Vodak, J. Wachter, M. O'Keeffe, O.M. Yaghi, Systematic design of pore size and functionality in isoreticular MOFs and their application in methane storage, Science 2002, 295, 469–472.
30. N. Stock, S. Biswas, Synthesis of Metal-Organic Frameworks MOFs.: Routes to Various MOF Topologies, Morphologies, and Composites, Chem Rev., 2012, 112, 933–969.
31. A. Car, C. Stropnik, K.-V. Peinemann, Hybrid membrane materials with different metal–organic frameworks MOFs. for gas separation, Desalination 2006, 200, 424–426.
32. T. Rodenas, M. van Dalen, P. Serra-Crespo, F. Kapteijn, J. Gascon, Mixed matrix membranes based on NH2-functionalized MIL-type MOFs: Influence of structural and operational parameters on the CO 2/CH4 separation performance, Microporous Mesoporous Mater. 2014, 192, 35–42.
33. Y. He, J. Shang, Q. Gu, G. Li, J. Li, R. Singh, P. Xiao, P.A. Webley, Converting 3D rigid metal-organic frameworks MOFs. to 2D flexible networks via ligand exchange for enhanced CO2/N2 and CH4/N2 separationChem Commun Camb. 201, 51, 14716–14719.
34. T. Zhang, W.B. Lin, Metal-organic frameworks for artificial photosynthesis and photocatalysis, Chem. Soc. Rev. 2014, 43, 5982–5993.
35. C.X. Chen, Z.W. Wei, J.J. Jiang, S.P. Zheng, H.P. Wang, Q.F. Qiu, C.C. Cao, D. Fenske, C.Y. Su, Dynamic Spacer Installation for Multirole Metal–Organic Frameworks: A New Direction toward Multifunctional MOFs Achieving Ultrahigh Methane Storage Working Capacity, J Am Chem Soc 139 2017. 6034–6037.
36. J. Della Rocca, D.M. Liu, W.B. Lin, Nanoscale Metal–Organic Frameworks for Biomedical Imaging and Drug Delivery, Acc. Chem. Res. 2011, 44, 957–968.
37. C.Y. Sun, C. Qin, X.L. Wang, Z.M. Su, Metal-organic frameworks as potential drug delivery systems, Expert Opin Drug Deliv 2013, 10, 89–101.
38. Z.C. Hu, B.J. Deibert, J. Li, Luminescent metal-organic frameworks for chemical sensing and explosive detection, Chem. Soc. Rev. 2014, 43, 5815–5840.
39. W.P. Lustig, S. Mukherjee, N.D. Rudd, A.V. Desai, J. Li, S.K. Ghosh, Metal-organic frameworks: Functional luminescent and photonic materials for sensing applications, Chem. Soc. Rev. 2017, 46, 3242–3285.
40. J.R. Li, R.J. Kuppler, H.C. Zhou, Selective gas adsorption and separation in metal–organic frameworks, Chem Soc Rev. 2009, 38, 1477–1504.
41. B. Van de Voorde, B. Bueken, J. Denayer, D. De Vos, Adsorptive separation on metal-organic frameworks in the liquid phase, Chem Soc Rev. 2014, 43, 5766–5788.
42. P.A. Kobielska, A.J. Howarth, O.K. Farha, S. Nayak, Metal–organic frameworks for heavy metal removal from water, Coord. Chem. Rev. 2018, 358, 92–107.
43. Elham Ragheb, Mojtaba Shamsipur, Fahimeh Jalali, Farimah Mousavi, Modified magnetic-metal organic framework as a green and efficient adsorbent for removal of heavy metals, Journal of Environmental Chemical Engineering, 2022, 102., 107297.
44. Hafezeh Nabipour, Sohrab Rohani, Sadia Batool, Adeyinka Sikiru Yusuff, An overview of the use of water-stable metal-organic frameworks in the removal of cadmium ion, Journal of Environmental Chemical Engineering, 2023, 111., 109131.
45. Guo Lin, Biao Zeng, Jing Li, Zeying Wang, Shixing Wang, Tu Hu, Libo Zhang, A systematic review of metal organic frameworks materials for heavy metal removal: Synthesis, applications and mechanism,Chemical Engineering Journal 2023, 460,141710.
46. Chakraborty, P., Yao, K.M., Chennuri, K. Krishna Vudamala, K. Raghunadh Babu, P. V., Interactions of mercury with different molecular weight fractions of humic substances in aquatic systems. Environ Earth Sci 2014, 72, 931–939.
47. A. K. Singha Deb, N. Dhume, K. Dasgupta, Sk. M. Ali, K. T. Shenoy, S. Mohan, Sulphur Ligand Functionalized Carbon Nanotubes for Removal of mercury from waste water – experimental and density functional theoretical study, Sep. Sci. Technol. 2019, 54, 1573-1587.
48. Zheng Yin, Shuang Wan, Jian Yang, Mohamedally Kurmoo, Ming-Hua Zeng,Recent advances in post-synthetic modification of metal–organic frameworks: New types and tandem reactions, Coordination Chemistry Reviews 2019, 378, 500-512.
49. Lien T.L. Nguyen, Tung T. Nguyen, Khoa D. Nguyen, Nam T.S. Phan,Metal–organic framework MOF-199 as an efficient heterogeneous catalyst for the aza-Michael reaction, Applied Catalysis A: General 2012, 425–426, 44-52.
50. B. Levasseur, C. Petit, T.J. Bandosz, Reactive adsorption of NO2 on copper-based metal-organic framework and graphite oxide/metal-organic framework composites, ACS Appl. Mater. Inter. 2010, 2, 3606–3613.
51. K. Schlichte, T. Kratzke, S. Kaskel, Improved synthesis, thermal stability and catalytic properties of the metal-organic framework compound Cu3BTC.2, Microporous Mesoporous Mater. 2004, 73, 81–88.
52. Gustafsson, M.; Bartoszewicz, A.; Martín-Matute, B.; Sun, J.; Grins, J.; Zhao, T.; Li, Z.; Zhu, G.; Zou, X. A Family of Highly Stable Lanthanide Metal-Organic Frameworks: Structural Evolution and Catalytic Activity. Chem. Mater. 2010, 22, 3316– 3322.
53. Y. Guo, X. Gao, C. Zhang, Y. Wu, X. Chang, T. Wang, X. Zheng, A. Du, B. Wang, J. Zheng, K. Ostrikov and X. Li, Plasma modification of a Ni-based metal-organic framework for efficient hydrogen evolution, J. Mater. Chem. A, 2019, 7, 8129–8135.
54. J. Limo, S. Lee, A. Sharma, J. Seong, S. B. Baek. M. S. Lah, Ligand functionalization of defect-engineered Ni-MOF-74, RSC Adv., 2022, 12, 31451-31455.
55. A. K. Das, R. S. Vemuri, I. Kutnyakov, B. P. McGrail, R. K. Motkuri, An Efficient Synthesis Strategy for Metal-Organic Frameworks: Dry-Gel Synthesis of MOF-74 Framework with High Yield and Improved Performance, Scientific Reports 2016, 6, 28050.
56. Worch, Eckhard. Adsorption Technology in Water Treatment: Fundamentals, Processes, and Modeling, Berlin, Boston: De Gruyter, 2012.
57. P. J. Lloyd-Jones, J. R. Rangel-Mendez, M. Streat, Mercury sorption from aqueous solution by chelating ion exchange resins, activated carbon and a biosorbent. Institution of Chemical Engineers: Part B: Process Safety and Environmental Protection 2004, 82(B4), 301-311.

	**Dr. Ashish Kumar Singha Deb** *presently working as a scientific officer in Chemical Engineering Division, Bhabha Atomic Research centre, after completion of one year orientation programme from 51st batch of BARC training school in 2008. He completed his PhD in from HBNI in 2019under the guidance of Prof. Musharaf Ali. His main area of research is the development of functionalized resins and nano-adsorbents for separation of metal ions and isotopes through DFT calculation and experimental studies. He is serving as a lab-in charge for quality control of sample analysis for elemental and isotopic measurements. He has 41publications in peer-reviewed journals, 43 in symposium and conferences, and 2 book chapters.*
	**Dr. Siddhartha Kolay** *has done his M. Sc. in Inorganic Chemistry from the University of Calcutta and joined the Chemistry Division, BARC, in 2007 after graduating from the 50th batch of the training school. He obtained his Ph.D. from Homi Bhabha National Institute, Mumbai, in 2016. His research work is primarily focused on the synthesis of metal-organic frameworks (MOFs) and covalent organic frameworks (COFs) for various applications. His current research interest is the development of radiation-stable MOFs and COFs for nuclear off-gas treatment and heavy metal extraction from nuclear waste.*
	**Smt. Manju Mohan** *is working in Atomistic Modeling and Chemical Analysis Section of Chemical Engineering Division, BARC. She is working on the development of functionalized carbon nano materials and MOFs for the separation of heavy metal ions. She has experience of quality control of sample analysis using various analytical instruments for elemental and isotopic determination. She has 7 peer-reviewed joiurnal, symposium and conference publications in her credit.*
	**Dr. Sk. Musharaf Ali**, *joined Chemical Engineering Division, after completion of one year orientation programme from 40th batch of training school in 1997. His main thrust of research is in the field of chemical product and process modeling using the density functional theory and MD simulations in collaboration with experimentalists. His research interests are structural, thermodynamical and dynamical aspects of inorganic and organic metal complexes in bulk, pores and at the interface using the tools of ab initio density functional theory and MD simulations. He has over 354 publications to his credit in journals, symposia and conferences and two book chapters. Presently, he is working on the design of nanoporous membranes for water purification and metallic membrane for gas permeation and computational glass vitrification for nuclear waste.*

SOCIETY FOR MATERIALS CHEMISTRY (SMC)

(Reg. No. - Maharashtra, Mumbai/1229/2008/GBBSD)
c/o Chemistry Division
Bhabha Atomic Research Centre, Mumbai 400085

APPLICATION FOR MEMBERSHIP

Please enroll me as a Life member of the Society for Materials Chemistry (SMC).
My particulars are as follows:

Name : _____

Educational Qualifications : _____

Field of Specialization : _____

_____

Official Address : _____

_____

Telephone No. (Off.) : _____

Residential Address : _____

_____

Telephone No. (Res.) : _____

Address for Correspondence : Home/Office (Please tick one of the options)

E-mail Address : _____

Subscription Details

Modeof Payment : Cheque/DD/Cash

(Cheque/DD should be drawn in favor of *"Society for Materials Chemistry"* for Rs. 1000/- payable at Mumbai. For out-station *non-multi-city* cheques, please include Rs.50/- as additional charge for bank clearance.

Number :

Dated :

Drawn on Bank & Branch :

Amount :

Place:

Date: Signature

Registration Number: _____ (To be allotted by SMC office)

Printed by:
Ebenezer Printing House
Unit No. 5 & 11, 2nd Floor, Hind Service Industries
Veer Savarkar Marg, Shivaji Park Sea-Face, Dadar (W), Mumbai - 400 028
Tel.: 2446 2632 / 2446 3872 Tel Fax: 2444 9765 E-mail: outworkeph@gmail.com

In this issue

Published by

Society for Materials Chemistry

C/o. Chemistry Division

Bhabha Atomic Research Centre, Trombay, Mumbai 40085

e-mail: socmatchem@gmail.com, Tel: 91-22-25592001